

Lévy-Rosenzweig-Porter random matrix ensemble

G. Biroli¹ and M. Tarzia^{2,3}¹Laboratoire de Physique de l'École Normale Supérieure, ENS, Université PSL, CNRS, Sorbonne Université, Université de Paris, F-75005 Paris, France²LPTMC, CNRS-UMR 7600, Sorbonne Université, 4 Pl. Jussieu, F-75005 Paris, France³Institut Universitaire de France, 1 Rue Descartes, 75231 Paris Cedex 05, France (Received 17 January 2021; revised 18 March 2021; accepted 19 March 2021; published 25 March 2021)

In this paper, we consider an extension of the Rosenzweig-Porter model, the Lévy-RP (L-RP) model, in which the off-diagonal matrix elements are broadly distributed, providing a more realistic benchmark to develop an effective description of nonergodic extended (NEE) states in interacting many-body disordered systems. We put forward a simple, general, and intuitive argument that allows one to unveil the multifractal structure of the minibands in the local spectrum when hybridization is due to anomalously large transition amplitudes in the tails of the distribution. The idea is that the energy spreading of the minibands can be determined self-consistently by requiring that the maximal hybridization rate \mathcal{H}_{ij} between a site i and the other N^{D_1} sites of the support set is of the same order of the Thouless energy itself N^{D_1-1} . This argument yields the fractal dimensions that characterize the statistics of the multifractal wave functions in the NEE phase, as well as the whole phase diagram of the L-RP ensemble. Its predictions are confirmed both analytically, by a thorough investigation of the self-consistent equation for the local density of states obtained using the cavity approach, and numerically, via extensive exact diagonalizations.

DOI: [10.1103/PhysRevB.103.104205](https://doi.org/10.1103/PhysRevB.103.104205)

I. INTRODUCTION

The appearance of nonergodic extended (NEE) eigenstates which are neither localized nor fully ergodic and occupy a subextensive part of the whole accessible Hilbert space has emerged as a fundamental property of many physical problems, including Anderson and many-body localization (MBL), random matrix theory, quantum information, and even quantum gravity. Multifractal one-particle wave functions have been proven to appear exactly at the transition point of the Anderson localization (AL) problem [1,2]. In the presence of interactions, although the existence of the MBL transition [3] is now well established, at least for one-dimensional systems (see also Ref. [4] and Refs. [5–9] for recent reviews), the investigation of NEE phases is far from being completed. On the one hand, recent numerical results [10–13] and perturbative calculations [14–16] strongly indicate that the many-body eigenstates are multifractal in the whole insulating regime. On the other hand, a subdiffusive behavior has often been found in the delocalized phase of such systems preceding the MBL transition [17,18], raising the possibility of the existence of a NEE regime also in the delocalized side of the phase diagram [19], as originally suggested in the seminal work of Ref. [20]. Strong indications in favor of such a phase, often nicknamed bad metal, have been recently reported in the out-of-equilibrium phase diagram of the quantum version of Derrida's random energy model [21–25], which can be thought of as the simplest mean-field quantum spin glass, and have been intensively discussed in the context of AL on hierarchical graphs [26–38]. The hierarchical, multifractal structure of eigenstates and hence of the local spectrum

(fractal minibands) in interacting qubit systems is also relevant in the context of quantum computation, since it is believed to play a key role in search algorithms based on efficient population transfer [39]. Finally, fractal eigenfunctions were recently observed and intensively investigated in the context of Josephson junction chains [40] and even in the Sachdev-Ye-Kitaev model of quantum gravity [41].

Although the existence of multifractal eigenstates is of principle importance in physical systems as it implies the breakdown of conventional Boltzmann statistics, the properties of the NEE phases, their analytic description, and the understanding of the physical mechanisms that produce them are still far from being well established.

Inspired by the success of random matrix theory, whose predictions are relevant in such seemingly different fields of physics [42,43], Kravtsov *et al.* proposed a solvable random matrix model [44], the generalized Rosenzweig-Porter (RP) model [45], in which fractal wave functions appear in an intermediate region of the phase diagram, sandwiched between the fully ergodic and the fully localized phases. The RP model has been intensively investigated over the past few years [46–56], as it provides a playground to explore the nature and the properties of NEE states. Nonetheless, the RP model is largely oversimplified: Differently from realistic many-body systems, the minibands in the local spectrum are fractal and not *multifractal*, the spectrum of fractal dimension is degenerate, and anomalously strong resonances are absent. In fact, in the RP model every site of the reference space, represented by a matrix index, is connected to every other site with the transition amplitude distributed according to the Gaussian law. In more realistic interacting models,

delocalization of the wave functions is due to a long series of quantum transitions and the effective transition rates between distant states in the Hilbert space are in general correlated and broadly distributed [13,16,57] due to the appearance of strong far-away resonances.

To overcome, at least partially, these issues and to formulate a more realistic effective description of the NEE phase, very recently an extension of the RP model, called the LN-RP ensemble, in which the off-diagonal matrix elements have a wide log-normal distribution, has been introduced and studied [58,59] (see Appendix C). In this paper, we consider another very natural generalization of the RP model with power-law distributed off-diagonal matrix elements, introduced in Ref. [53], which we dub the Lévy-Rosenzweig-Porter (L-RP) ensemble. Differently from the Gaussian RP case, hybridization of the energy levels in the L-RP ensemble can be produced by anomalously large transition amplitudes in the tails of the distribution which cannot be described by perturbation theory (see Appendix E).

We present two complementary strategies which circumvent this difficulty. These strategies are able to take into account the effect of the broadly distributed off-diagonal matrix elements in a self-consistent way and to unveil the multifractal statistics of the eigenstates.

The first strategy consists of a very simple and physically intuitive extreme value statistics argument: The idea is that the size of the support set of the minibands in the local spectrum, N^{D_1} , can be determined self-consistently by requiring that the largest hopping amplitudes between a site i and the other N^{D_1} sites belonging to the same support set are of the same order of the energy spreading of the miniband itself, $E_{Th} \propto N^{D_1-1}$. The second strategy is based on the cavity equations for the resolvent, which become asymptotically exact in the thermodynamic limit, providing a way to resume the whole perturbative series in a self-consistent way. Within this framework, the multifractal statistics can be directly accessed by computing analytically the asymptotic scaling behavior of the typical value of the local density of states (LDoS) in the NEE regime. These two approaches give exactly the same predictions for the phase diagram of the L-RP ensemble as a function of the parameters μ (which characterize the exponent of the tails of the distribution of the transition amplitudes) and γ (which characterize the scaling of their typical value with the system size N), as well as for the anomalous dimensions of the eigenstates in the NEE phase.

We complement these results by extensive exact diagonalizations which confirm the theoretical analysis and allows one to investigate in great detail the properties of the phase transitions between the ergodic, NEE, and AL phases. Our results for the Thouless energy (and thus for the boundaries of the NEE phase) coincide with the ones obtained in Ref. [53] within the Wigner-Weisskopf approximation for $1 < \mu < 2$. In the present paper, we complete the study of the model by providing detailed results on several observables related to the level statistics, the statistics of the wave functions's amplitudes, and the statistics of the LDoS in all the regions of the phase diagram.

The rest of the paper is organized as follows: In the next section, we define the model. In Sec. III, we put forward a physically transparent argument that allows one to determine

the multifractal structure of the minibands and the anomalous dimensions of the eigenstates in the NEE phase, as well as the phase diagram of the L-RP ensemble. In Sec. IV, we discuss simple rule of thumb criteria for localization and ergodicity of a dense random matrix with uncorrelated entries recently formulated in Refs. [48,58–60]. In Sec. V, we investigate the statistics of the local resolvent by means of the cavity approach which fully supports the results presented in the previous sections. In Sec. VI, we compare the analytical predictions for the fractal exponents with extensive numerical simulations. In Secs. VII and VIII, we investigate numerically the behavior of the level statistics and of the spectral correlation functions, showing that they are in full agreement with the theoretical analysis. Finally, in Sec. IX, we present some concluding remarks and perspectives for future investigations. In the Appendixes, we present some supplementary information that complements the results discussed in the main text, as well as some technical aspects.

II. THE MODEL

We consider a natural modification of the RP ensemble [53] where the independent and identically distributed (i.i.d.) off-diagonal elements are taken from a Lévy distribution with power-law tails [61–70]. The Hamiltonian of the L-RP model is a sum of two independent $N \times N$ matrices,

$$\mathcal{H} = \mathcal{A} + \kappa \mathcal{L}_{\mu,\gamma}, \quad (1)$$

where $\mathcal{A}_{ij} = \epsilon_i \delta_{ij}$ is a diagonal matrix with i.i.d. random entries taken from a given distribution of width W (our results are independent of its specific form [71]), and $\mathcal{L}_{\mu,\gamma}$ is a Lévy matrix with i.i.d. broadly distributed elements with a power-law tail of exponent $1 + \mu$ and typical value of the order $N^{-\gamma/\mu}$. κ is a constant of $O(1)$. For concreteness, one can take a Student distribution which reads

$$P_{\mu,\gamma}(\mathcal{L}_{ij}) = \frac{\mu}{2N^\gamma \mathcal{L}_{ij}^{1+\mu}} \theta(|\mathcal{L}_{ij}| > N^{-\gamma/\mu}). \quad (2)$$

The largest elements of each row or column of $\mathcal{L}_{\mu,\gamma}$ are of order $N^{(1-\gamma)/\mu}$. Hence, they are much smaller than W for any $\gamma > 1$ (while the largest element of the whole $N \times N$ matrix is of order $N^{(2-\gamma)/\mu}$, which is much smaller than W only for $\gamma > 2$). The average DoS of \mathcal{H} is thus given by the DoS of \mathcal{A} , $\rho(E) \simeq p(E)$, for $\gamma > 1$ in the thermodynamic limit (except a vanishing fraction of eigenvalues of energy of order $N^{(2-\gamma)/\mu}$ in the Lifshitz tails of the spectrum). For $\gamma < 1$, it is instead given by the DoS of Lévy matrices (which can be computed exactly [63]) but with eigenvalues proportional to $N^{(1-\gamma)/\mu}$. The standard RP model is recovered for $\mu = 2^+$ [44,47], when the variance of the \mathcal{L}_{ij} 's is finite and the off-diagonal matrix belongs to the Gaussian Orthogonal Ensemble (GOE), with the typical value scaling as $[\mathcal{L}_{ij}]_{\text{typ}} \sim N^{-\gamma/2}$. For $\mu > 2$, the average DoS is thus given by $p(E)$ for $\gamma > \mu/2$ and by the semicircle law for $\gamma < \mu/2$, with all eigenvalues rescaled by $N^{(\mu-2\gamma)/(2\mu)}$. In summary, in the bulk of the spectrum, the mean level spacing Δ is

$$\Delta \simeq \begin{cases} WN^{-1} & \text{for } \mu < 2 \text{ and } \gamma > 1 \\ \kappa N^{(1-\gamma-\mu)/\mu} & \text{for } \mu < 2 \text{ and } \gamma < 1 \\ WN^{-1} & \text{for } \mu > 2 \text{ and } \gamma > \mu/2 \\ \kappa N^{-(2\gamma+\mu)/(2\mu)} & \text{for } \mu > 2 \text{ and } \gamma < \mu/2. \end{cases} \quad (3)$$

Since Lévy matrices play a central role in the L-RP model, let us recall the main results. Lévy matrices (corresponding to $W = 0$, $\mu < 2$, and $\gamma = 1$) have been intensively investigated in the last few years both from the mathematical and the physical sides [61–70,72,73], since they represent a very broad universality class, with different and somehow unexpected properties compared to the Gaussian case. Their phase diagram turns out to be quite rich [61,62,65]: For $\mu > 1$, all eigenvalues in the bulk are fully delocalized and the level statistics is described by the GOE ensemble on the scale of the mean level spacing. There is, however, a small sub-extensive fraction of localized eigenvectors corresponding to the $N^{3/(2+\mu)}$ largest eigenvalues in the tails of the spectrum [66]. For $\mu < 1$, instead, a mobility edge appears at finite energy, separating extended eigenstates of energy $E < E_{\text{loc}}(\mu)$ from localized eigenstates of energy $E > E_{\text{loc}}(\mu)$. The statistics of neighboring levels is described by the GOE ensemble for $E < E_{\text{loc}}(\mu)$ and by Poisson statistics for $E > E_{\text{loc}}(\mu)$. The localization transition taking place at E_{loc} shares all the properties of AL in the tight-binding Anderson model on the Bethe lattice [37,38,74,75]. As shown in Ref. [62], the mobility edge can be computed analytically. $E_{\text{loc}}(\mu)$ does not depend on N in the thermodynamic limit for the natural scaling of the off-diagonal elements $\gamma = 1$ and tend to 0 for $\mu \rightarrow 0$ and diverges for $\mu \rightarrow 1^-$. With the scaling of Eq. (1), the mobility edge found for $0 < \mu < 1$ thus moves to energies of the order $N^{(1-\gamma)/\mu}$.

III. PHASE DIAGRAM OF THE L-RP ENSEMBLE

As first shown in Ref. [44] and later further discussed in Refs. [46–50], the RP random matrix model with diagonal disorder of width W and off-diagonal i.i.d. Gaussian elements of variance $N^{-\gamma}$ has three phases: fully ergodic for $\gamma < 1$, NEE for $1 < \gamma < 2$, and fully localized for $\gamma > 2$, and two transitions between them at $\gamma_{\text{ergo}} = 1$ and $\gamma_{\text{AL}} = 2$. The same kind of phases and transitions between them are expected for the L-RP model [53].

To proceed further, let us first recall that the smoking gun evidence [44,47,48] of the NEE phase is the presence of the minibands in the local spectrum: Eigenstates occupy a subextensive fraction of the total volume and spread over N^{D_1} consecutive energy levels which are hybridized by the off-diagonal perturbation, while wave functions belonging to different support sets do not overlap in the thermodynamic limit. In the Gaussian RP model, the width of the minibands, called the Thouless energy, is given by $E_{\text{Th}} \propto \Gamma_{\text{av}} = 2\pi \rho N \langle |\mathcal{H}_{ij}|^2 \rangle$, which is, according to Fermi's golden rule (FGR), the average escape rate of a particle at a given site i (ρ is the average DoS of \mathcal{H} , see Sec. IV for more details). In the NEE phase ($1 < \gamma < 2$), one has that $E_{\text{Th}} \sim N^{1-\gamma}$, with $\Delta \ll E_{\text{Th}} \ll W$. On the other hand, the Thouless energy must also be equal to the number of sites of a support set occupied by an eigenstate, N^{D_1} , times the average distance between consecutive levels, $\Delta \sim N^{-1}$, implying that $D_1 = 2 - \gamma$. As anticipated in the Introduction, the minibands in the Gaussian RP model are *fractal* (and not *multifractal*) and the anomalous dimensions are not degenerate ($D_q = D \forall q > 1/2$).

Below we illustrate a very simple, general, and physically transparent argument that yields E_{Th} and D_1 when

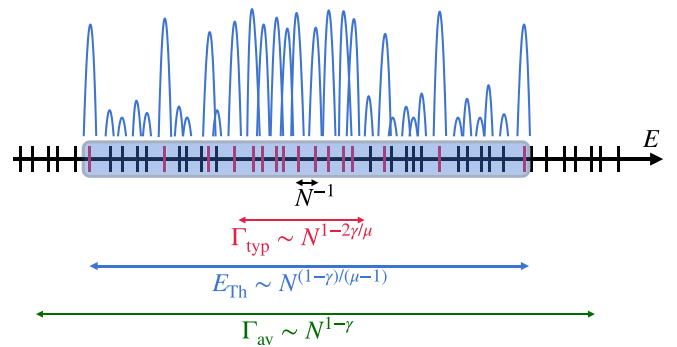


FIG. 1. Pictorial representation of the fractal structure of the minibands and of a wave function belonging to it for $1 < \mu < 2$ and $1 < \gamma < \mu$. Consecutive levels are in resonance due to typical off-diagonal matrix elements. However, the minibands extend to a much larger energy scale due to rare resonances produced by anomalously large matrix elements. The energy spreading E_{Th} of the minibands is determined self-consistently by asking that the maximum hybridization gap \mathcal{L}_{ij} of E_{Th}/N^{-1} adjacent levels has the same scaling of the width of the minibands itself, Eq. (4), and is much smaller than the average effective bandwidth Γ_{av} found from standard perturbation theory.

hybridization occurs on an energy scale much larger than Γ_{typ} due to anomalously large matrix elements in the tail of the distribution (see Fig. 1 for a pictorial illustration of this argument). Besides the structure of the minibands in the NEE phase and the anomalous dimensions which characterize the statistics of the amplitudes of the multifractal wave functions, this argument also yields the phase diagram of the L-RP ensemble. These predictions will then be confirmed in the next sections both analytically, by a thorough analysis of the cavity equations, and numerically, by means of extensive exact diagonalizations.

Let us focus on the case $\mu < 2$ and $\gamma > 1$ and let us assume that in the NEE phase the minibands contain N^{D_1} energy levels and thus extend up to an energy scale of $E_{\text{Th}} = N^{D_1} \times N^{-1}$. Let us consider a site i belonging to a given miniband. Hybridization of i with the N^{D_1} levels j of the support set is only possible if the maximum of the off-diagonal matrix elements \mathcal{H}_{ij} among those levels, which scales as $N^{D_1/\mu-\gamma/\mu}$, is of the same order of the width of the miniband itself:

$$E_{\text{Th}} \sim N^{D_1-1} \sim \max_{j=1,\dots,N^{D_1}} \{\mathcal{H}_{ij}\} \sim N^{D_1/\mu-\gamma/\mu}. \quad (4)$$

Hence, in the NEE phase, one must have $D_1 = (\mu - \gamma)/(\mu - 1)$ and $E_{\text{Th}} \sim N^{(1-\gamma)/(\mu-1)}$. (The expression found for E_{Th} is in fact in agreement with the one of Ref. [53], although it is has been obtained with a different approach. Conversely the approximations of Ref. [53] do not lead to the correct result for the fractal dimensions, which were predicted to be equal to zero for all $q > \mu/2$.)

AL occurs when the minibands' width formally becomes smaller than the mean-level spacing. At this point, which corresponds to $E_{\text{Th}} \sim N^{-1}$, i.e., $\gamma_{\text{AL}} = \mu$ for $\mu > 1$ [53], the levels of \mathcal{A} are almost unaffected by the Levy perturbation. Conversely, ergodicity is restored when the Thouless energy becomes of the order of the total spectral bandwidth, $E_{\text{Th}} \sim W$, i.e., $\gamma_{\text{ergo}} = 1$ [53].

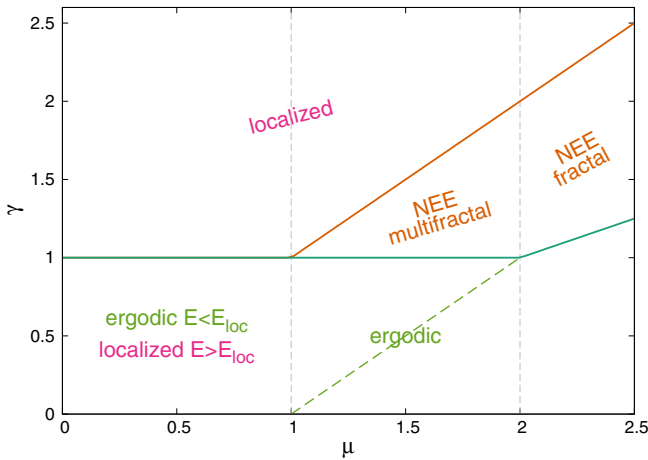


FIG. 2. Phase diagram of the L-RP ensemble. The transition lines to the AL phase γ_{AL} and to the ergodic phase γ_{ergo} are given in Eq. (5). For $\mu > 2$, the NEE phase becomes fractal (and not multifractal). As shown in Ref. [62], for $\mu < 1$ and $\gamma < 1$, a mobility edge separates a delocalized phase for $E < E_{\text{loc}}$ from an Anderson localized phase for $E > E_{\text{loc}}$ with $E_{\text{loc}} \sim N^{(1-\gamma)/\mu}$ with the scaling of Eq. (2). The green dashed line separates a weakly ergodic regime, ($\mu < 1$, $E < E_{\text{loc}}$) and ($1 < \mu < 2$, $\gamma > \mu - 1$), similar to the metallic phase of the Anderson model (see Sec. IV and Ref. [59] for its definition), from a fully ergodic one ($1 < \mu < 2$, $\gamma < \mu - 1$) and ($\mu > 2$, $\gamma < \mu/2$), where the orthogonal symmetry fully establishes.

For $\mu \rightarrow 2$, one recovers the RP result, $E_{\text{Th}} \sim N^{1-\gamma}$, and the Thouless energy becomes equal to the typical effective bandwidth. For $\mu > 2$, one thus has that $E_{\text{Th}} \sim \Gamma_{\text{typ}} \sim N^{1-2\gamma/\mu}$ and $D_1 = 2 - 2\gamma/\mu$. At the AL transition $E_{\text{Th}} \sim \Delta$ [given in Eq. (3)], i.e., $\gamma_{\text{AL}} = \mu$, while ergodicity is fully restored when $E_{\text{Th}} \sim W$, i.e., $\gamma_{\text{ergo}} = \mu/2$. The resulting phase diagram of the L-RP ensemble is reported in Fig. 2, and the transition lines between the different phases are

$$\gamma_{\text{ergo}} = \begin{cases} 1 & \text{for } \mu \leq 2 \\ \mu/2 & \text{for } \mu > 2, \end{cases} \quad \gamma_{\text{AL}} = \begin{cases} 1 & \text{for } \mu \leq 1 \\ \mu & \text{for } \mu > 1. \end{cases} \quad (5)$$

This analysis predicts the existence of a tricritical point (similarly to the LN-RP ensemble [58,59]) for $\mu = 1$ (i.e., Cauchy distributed off-diagonal elements [70]) and $\gamma = 1$. We will come back to the peculiar properties of such a tricritical point in the next sections.

In the larger N limit, the spectral dimension D_1 is thus given by

$$D_1(\gamma) = \begin{cases} 1 & \text{for } \gamma \leq \gamma_{\text{ergo}} \\ \frac{\mu-\gamma}{\mu-1} & \text{for } \mu < 2 \text{ and } \gamma_{\text{ergo}} < \gamma \leq \gamma_{\text{AL}} \\ 2 - \frac{2\gamma}{\mu} & \text{for } \mu > 2 \text{ and } \gamma_{\text{ergo}} < \gamma \leq \gamma_{\text{AL}} \\ 0 & \text{for } \gamma > \gamma_{\text{AL}}, \end{cases} \quad (6)$$

implying that D_1 is continuous for $\mu > 1$ both at the transition to the NEE phase ($D_1 \rightarrow 1$ for $\gamma \rightarrow \gamma_{\text{ergo}}^+$) and at the Anderson transition ($D_1 \rightarrow 0$ for $\gamma \rightarrow \gamma_{\text{AL}}^-$). For $\mu \leq 1$, instead D_1 is expected to display a discontinuous jump from $D_1 = 1$ for $\gamma = 1$ to $D_1 = 0$ for $\gamma = 1^+$ [76].

The argument illustrated above also suggests that higher order moments of the wave functions' amplitudes exhibit a different scaling with N , and hence that the fractal dimensions

are not degenerate. In particular, the anomalous dimension D_∞ , associated with the scaling of the number of sites where the amplitudes take the largest values, should be dominated by the compact part of the support set of the eigenstates. In fact, most of the sites where the wave functions' amplitudes are large falls within the typical bandwidth and only a few of them (i.e., a subextensive fraction of the N^{D_1} sites of the support set) are outside it (see Fig. 1). On most of the sites of the miniband at energy separation larger than Γ_{typ} , the amplitudes are typically smaller since these sites are only hybridized at higher orders in perturbation theory. One thus has

$$D_\infty(\gamma) = \begin{cases} 1 & \text{for } \gamma \leq \gamma_{\text{ergo}} \\ 2 - \frac{2\gamma}{\mu} & \text{for } \gamma_{\text{ergo}} < \gamma \leq \gamma_{\text{AL}} \\ 0 & \text{for } \gamma > \gamma_{\text{AL}}. \end{cases} \quad (7)$$

This implies that D_∞ should display a finite jump at the ergodic transition for $\mu < 2$. The amplitude of the jump is $1 - 2/\mu$ and goes to one for $\mu \rightarrow 1$ and to zero in the RP limit, $\mu \rightarrow 2$. The difference between D_1 and D_∞ confirms that the L-RP ensemble displays *multifractal* behavior, contrary to the Gaussian RP model. In the latter, one has that $\langle |\mathcal{H}_{ij}|^2 \rangle = [\mathcal{H}_{ij}]_{\text{typ}}^2$, implying that the *average* effective spectral bandwidth coincides with the *typical* one. This is, of course, not the case for the L-RP ensemble, since the matrix elements are broadly distributed and $\Gamma_{\text{av}} \neq \Gamma_{\text{typ}}$ for $\mu < 2$.

Note that since neighboring energy levels are always hybridized by the off-diagonal terms, the level statistics on the scale of the mean-level spacings is expected to be described by the GOE ensemble in the whole NEE phase, as for the Gaussian RP model. In Secs. V–VIII, we will present a thorough analytical and numerical investigation of the L-RP model that fully confirms the predictions of Eqs. (5)–(7), while in the next section we show that the phase diagram of Fig. 2 is in agreement with the simple rule of thumb criteria for localization and ergodicity of dense random matrices with uncorrelated entries recently formulated in Refs. [48,58–60]. In Appendix E, we show that in the AL phase, where perturbation theory converges absolutely, one can determine the whole spectrum of fractal dimensions exactly, Eq. (E3).

Note, however, that the argument presented above does not take into account the spectral properties of the off-diagonal Lévy perturbation. In fact, as explained in Sec. II, for $\mu < 1$ a mobility edge appears in the spectrum of Lévy matrices, separating fully extended eigenstates of energy $E < E_{\text{loc}}(\mu)$ from AL eigenstates of energy $E > E_{\text{loc}}(\mu)$ [62,65]. For $\gamma = 1$, the mobility edge $E_{\text{loc}}(\mu)$ is finite and does not depend on N in the thermodynamic limit ($E_{\text{loc}}(\mu)$ tends to 0 for $\mu \rightarrow 0$ and diverges for $\mu \rightarrow 1^-$ [62]). With the scaling of Eq. (1), the mobility edge thus moves to energies of the order $N^{(1-\gamma)/\mu}$. Since the rare large off-diagonal elements which are responsible for the hybridization of the energy levels are in fact associated to strongly localized eigenfunctions, one expects that for $\mu < 1$ and $\gamma < 1$ the system is delocalized at low energy and localized at high energy, with a mobility edge scaling as $N^{(1-\gamma)/\mu}$. We will study this region of the phase diagram in Appendix A.

The other aspect that the argument might not take into account is that, as recently shown in Ref. [59], the multifractal states might be fragile against hybridization and the NEE

phase could be in fact be squeezed due to this effect. We will investigate this possibility in Appendix B, showing that for the L-RP ensemble such instability does not take place.

We would like to stress the fact that the argument presented in this section is very general and physically transparent and can in principle be extended to analyze the multifractal states in other systems. The same kinds of ideas and reasoning might be reformulated and adapted to situations in which the matrix elements are correlated [60] and/or depend on the matrix indices and on the energy separation, as in more realistic interacting models [13,16,23]. As an illustration, in Appendix C we show that applying these ideas to the LN-RP ensemble of Refs. [58,59] allows one to obtain the phase diagram and the anomalous dimensions of the model in a few lines of calculation.

IV. SIMPLE RULE OF THUMB CRITERIA FOR LOCALIZATION AND ERGODICITY

In this section, we apply the rule of thumb criteria for localization and ergodicity of a dense random matrix with uncorrelated entries recently formulated in Refs. [48,58–60], showing that they yield an estimation of the phase diagram of the L-RP ensemble and of the transition lines between the different phases which are in full agreement with Fig. 2 and Eq. (5).

The first criterion [48,58–60] states that AL occurs when the sum

$$\lim_{N \rightarrow \infty} \sum_{j=1}^N \langle |\mathcal{H}_{ij}| \rangle < \infty. \quad (8)$$

The physical interpretation of this condition is that if the number of sites j in resonance with a given site i is finite in the thermodynamic limit, then the system is localized.

The second criterion [48,58–60] is a sufficient condition of ergodicity. It states that if the sum

$$\lim_{N \rightarrow \infty} \sum_{j=1}^N \langle |\mathcal{H}_{ij}|^2 \rangle \rightarrow \infty, \quad (9)$$

the system is ergodic. Its physical interpretation is obtained by recalling that, according to Fermi's golden rule, the spreading amplitude

$$\Gamma_i \approx 2\pi \rho \sum_j |\mathcal{H}_{ij}|^2 \quad (10)$$

quantifies the escape rate of a particle created at a given site i , where ρ is the average DoS of \mathcal{H} . For $\mu < 2$ and $\gamma > 1$, one can neglect the contribution of off-diagonal matrix elements to the density of states and $\rho(E) \simeq p(E)$, and the total spectral bandwidth is limited by W . The condition Eq. (9) thus states that when the average spreading width Γ_{av} is much larger than the spread of energy levels $W \sim O(1)$ due to disorder, then the system is in the ergodic phase since starting from a given site the wave packet spreads to any other given site in times of order one. In other words, the fulfillment of this condition implies that there are no minibands in the local spectrum. [For $\gamma < 1$ and $\mu < 2$ or $\gamma < \mu/2$ and $\mu > 2$ instead, $\Gamma_{\text{av}} \gg W$

and the total spectral bandwidth $B = N\Delta$ is given by the off-diagonal matrix elements [62], see Eq. (3).]

The NEE phase is thus realized if

$$\lim_{N \rightarrow \infty} \sum_{j=1}^N \langle |\mathcal{H}_{ij}| \rangle \rightarrow \infty \quad \text{and} \quad \lim_{N \rightarrow \infty} \sum_{j=1}^N \langle |\mathcal{H}_{ij}|^2 \rangle \rightarrow 0.$$

For Lévy distributed off-diagonal elements, the second moment of $|\mathcal{H}_{ij}|$ diverges for any $\mu < 2$ and the first moment diverges for any $\mu < 1$. However, the averages appearing in Eqs. (8) and (9) should be done with the distribution truncated at the total spectral bandwidth $B = N\Delta$ [where Δ is given in Eq. (3)].

The reason for that is that rare large matrix elements $|\mathcal{H}_{ij}| \gg B$ split the resonance pair of levels so much that they are pushed at the Lifshitz tail of the spectrum and do not affect statistics of states in its bulk [58,59]. We thus have that

$$\langle |\mathcal{H}_{ij}|^q \rangle_B \sim \begin{cases} \frac{\mu \kappa^q}{\mu - q} N^{-\gamma q / \mu} & \text{for } q < \mu \\ \gamma \kappa^q N^{-\gamma} \ln N & \text{for } q = \mu \\ \frac{\mu \kappa^q B^{q-\mu}}{q-\mu} N^{-\gamma} & \text{for } q > \mu. \end{cases}$$

Applying the criteria Eqs. (8) and (9), one thus immediately recovers the phase diagram of Fig. 2 and the transition lines given in Eq. (5). Note that at the tricritical point ($\mu = 1$, $\gamma = 1$), one has that $N \langle |\mathcal{H}_{ij}| \rangle_W \sim \ln N \rightarrow \infty$ and $N \langle \mathcal{H}_{ij}^2 \rangle_W \sim W$. Hence the tricritical point is in the delocalized phase and should be characterized by a very weak ergodicity (wave functions occupy a finite fraction of the total Hilbert space). On the line of critical points at $\gamma = 1$ for $0 < \mu < 1$, both $N \langle |\mathcal{H}_{ij}| \rangle_W$ and $N \langle \mathcal{H}_{ij}^2 \rangle_W$ are finite and μ dependent with the ratio $\langle |\mathcal{H}_{ij}| \rangle_W / \langle \mathcal{H}_{ij}^2 \rangle_W \rightarrow \infty$ for $\mu \rightarrow 1$. Similarly, on the line of critical points separating the ergodic regime from the NEE one at $\gamma = 1$ and $1 < \mu < 2$, one has that $N \langle |\mathcal{H}_{ij}| \rangle_W \sim N^{1-1/\mu} \rightarrow \infty$ while $N \langle \mathcal{H}_{ij}^2 \rangle_W \sim W^{2-\mu} / (2-\mu)$. Hence such a critical line is in the ergodic phase and should be characterized by $D_q = 1$.

Although the criteria Eqs. (8) and (9) are originally based on first- and second-order perturbation theory for the eigenvectors and the eigenvalues, they give the correct results for the transition lines of the L-RP ensemble. Nevertheless, as discussed above, differently from the Gaussian RP counterpart, $N \langle \mathcal{H}_{ij}^2 \rangle_B$ does not necessarily coincide with $N \langle |\mathcal{H}_{ij}| \rangle_B^2$ due to the heavy tails of the distribution of the transition amplitudes. This property has several important consequences:

(1) The first implication is that the energy band Γ_{av} obtained from the FGR, which corresponds to the average spreading of the energy levels due to the off-diagonal perturbation, can be much larger than the mean level spacing in the AL phase. In fact, for $\mu < 2$ and $\gamma_{\text{AL}} < \gamma < 2$, one has that $\Gamma_{\text{av}} \gg N^{-1}$. In particular, on the transition line $\gamma = \mu$ for $1 < \mu < 2$, one finds that $N \langle \mathcal{H}_{ij}^2 \rangle_W \sim N^{1-\mu}$, while on the transition line $\gamma = 1$ for $0 < \mu < 1$ one finds that $N \langle \mathcal{H}_{ij}^2 \rangle_W \sim O(1)$. This is a clear manifestation of the failure of the perturbative expansion (see Appendix E for more details): Although the energy levels are scrambled by the matrix $\mathcal{L}_{\mu,\gamma}$ by a huge amount compared to Δ , the system is nevertheless localized due to the fact that different eigenstates do not overlap and cross each other without interacting.

(2) A second consequence, already anticipated above and further discussed in Secs. V and VI, is the fact that the typical escape rate $\Gamma_{\text{typ}} \approx 2\pi\rho N[\mathcal{H}_{ij}]_{\text{typ}}^2 \sim N^{1-2\gamma/\mu}$ does not coincide with the average one $\Gamma_{\text{av}} \sim N^{1-\gamma}$ for $\mu < 2$. This means that the *typical* energy band hybridized by the off-diagonal perturbation is much smaller than the *average* spreading width, which is a clear signature of the multifractality of the minibands in the NEE phase (see Fig. 1).

(3) Finally, the fact that $\Gamma_{\text{typ}} \neq \Gamma_{\text{av}}$ also has some implications on the properties of the ergodic phases led the authors of Ref. [59] to put forward an extra sufficient criterion for full ergodicity, which states that it is realized if

$$\lim_{N \rightarrow \infty} \frac{(N[\mathcal{H}_{ij}]_{\text{typ}}^2)^2}{N\langle |\mathcal{H}_{ij}|^2 \rangle_B} \rightarrow \infty. \quad (11)$$

If this condition is not fulfilled, the eigenfunction statistics is not invariant under basis rotation and the Wigner-Dyson statistics only establishes up to a finite energy scale, corresponding to a weakly ergodic phase in which the typical DoS is smaller than the average DoS. This is, for instance, what happens in the ergodic phase of Lévy matrices [62] or in the metallic phases of the Anderson model in three dimensions [77,78] and on the Bethe lattice [37,38], in which the Thouless energy is finite but strictly smaller than the total spectral bandwidth and the GOE statistics only establishes up to an energy scale of $O(1)$. Conversely, if Eq. (11) is verified, i.e., $\mu > 2$ and $\gamma < \mu/2$ or $1 < \mu < 2$ and $\gamma < \mu - 1$, the rotation invariance of the GOE ensemble fully establishes in the ergodic phase.

V. CAVITY EQUATIONS AND LOCAL RESOLVENT STATISTICS

Using the cavity method (or, equivalently, the block matrix inversion formula), it is possible to derive the equations relating the probability distribution of the diagonal elements of the resolvent of matrices of size $N + 1$ to those of size N [47,48,61,62,65]. In the large N limit, these equations become asymptotically exact and read:

$$[\mathcal{G}_{ii}^{(N+1)}]^{-1} = \epsilon_i - E - i\eta - \sum_{j=1}^N \mathcal{L}_{ij}^2 \mathcal{G}_{jj}^{(N)}. \quad (12)$$

In Ref. [47], it was shown that the existence of the NEE phase of the standard RP model can be revealed studying a nonstandard scaling limit in which the small additional imaginary regulator η vanishes as $N^{-\delta}$. At the Thouless energy E_{Th} —which is proportional to the typical level spacing, N^{-1} , times the number of sites, N^{D_1} , over which the eigenvectors are delocalized—the spectral statistics displays a crossover from a behavior characteristic of standard localized phases to a behavior similar to the one of standard delocalized phases. Thus, inspecting the local resolvent statistics one has a direct access to the nonergodic properties of the delocalized phase.

In the following, we carry out a similar analysis for the L-RP ensemble, focusing on the region $\mu < 2$ of the phase diagram (the case $\mu > 2$ is analogous to the one discussed in Refs. [47,48]). We focus on the imaginary part of the Green's function and drop the N dependence in Eq. (12) since one

can assume that in the thermodynamic limit the distribution of $\mathcal{G}^{(N+1)}$ is the same as the distribution of $\mathcal{G}^{(N)}$.

The matrix elements \mathcal{L}_{ij} and the elements of the resolvent are by construction uncorrelated. In the Gaussian RP case [47,48] from the central limit theorem, one has that the imaginary part of the self-energy,

$$S_i(z) = \sum_{j=1}^N \mathcal{L}_{ij}^2 \text{Im}\mathcal{G}_{jj}(z),$$

(with $z = E - i\eta$) is a Gaussian variable whose expectation value is given by $\pi\rho(E)N^{1-\gamma}$, where $\rho(E) \simeq p(E)$ is the average DoS. The scaling of the self-energy thus sets the scale of the Thouless energy, $E_{\text{Th}} \propto N^{1-\gamma}$, on which the crossover from localizedlike behavior (for $\eta \gg N^{1-\gamma}$) to delocalizedlike behavior (for $\eta \ll N^{1-\gamma}$) takes place [47].

The situation is, however, more involved in the L-RP case, where the \mathcal{L}_{ij}^2 's are broadly distributed. Using the generalized central limit theorem one finds that $S_i(z)$ is a Lévy distributed random variable with power-law tails with an exponent $1 + \mu/2$ and typical value given by

$$\text{typ} = N^{\frac{2(1-\gamma)}{\mu}} [\langle |\text{Im}\mathcal{G}(z)|^{\frac{\mu}{2}} \rangle]^{\frac{2}{\mu}}. \quad (13)$$

Hence, the typical value of the self-energy is related to the $(\mu/2)$ th moment of the Green's function and must be determined self-consistently, as explained in the following. Neglecting the real part of the resolvent (by using the same arguments as the ones given below one can, in fact, show that the real parts only give a subleading contribution) we get

$$\text{Im}\mathcal{G}_{ii}(z) \simeq \frac{\eta + S_i(z)}{[E - \epsilon_i]^2 + [\eta + S_i(z)]^2}. \quad (14)$$

Let us imagine a situation in which $\eta \gg S_i$:

$$\text{Im}\mathcal{G}_{ii} \simeq \begin{cases} \frac{\eta}{(E - \epsilon_i)^2} & \text{if } |E - \epsilon_i| \gg \eta \\ \frac{1}{\eta} & \text{if } |E - \epsilon_i| \ll \eta. \end{cases}$$

For N large and η small and fixed (but much larger than the S_i 's), one then recovers the standard localized behavior,

$$P(\text{Im}\mathcal{G}) \propto p(E) \frac{\sqrt{\eta}}{(\text{Im}\mathcal{G})^{3/2}}, \quad (15)$$

with a cutoff at $\text{Im}\mathcal{G} = 1/\eta$. For $\mu > 1$, we then have

$$\langle |\text{Im}\mathcal{G}|^{\frac{\mu}{2}} \rangle \propto \frac{\eta^{1-\frac{\mu}{2}}}{\mu - 1}. \quad (16)$$

In fact, the $\mu/2$ th moment of $\text{Im}\mathcal{G}$ is dominated by the upper cutoff of the distribution for $\mu > 1$ and is given by $(1/\eta)^{\mu/2}$ times the probability to find a resonance such that $|E - \epsilon_i| < \eta$, which is proportional to η . For $\mu < 1$, instead, $\langle |\text{Im}\mathcal{G}|^{\frac{\mu}{2}} \rangle \propto \eta^{\mu/2}$, and S_i is always negligible with respect to η in the denominator of Eq. (14) as soon as $\gamma > 1$. The system is then in the AL phase for $\mu < 1$ and $\gamma > 1$, in agreement with the results given in the previous section and illustrated in the phase diagram of Fig. 2. Hence, in the following we will focus on the range $1 < \mu < 2$ only.

Let us consider now the sites where $S_i \gg \eta$, where

$$\text{Im}\mathcal{G}_{ii} \simeq \begin{cases} \frac{S_i}{(E - \epsilon_i)^2} & \text{if } |E - \epsilon_i| \gg S_i \\ \frac{1}{S_i} & \text{if } |E - \epsilon_i| \ll S_i. \end{cases}$$

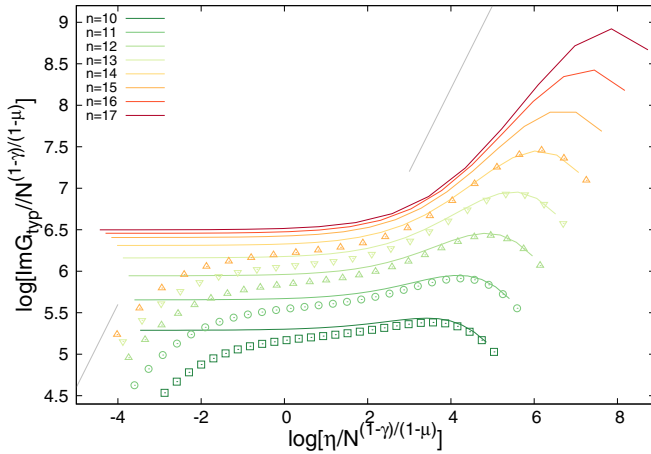


FIG. 3. $\text{Im}\mathcal{G}_{\text{typ}}$ as a function of the imaginary regulator η for several system sizes $N = 2^n$ (with n from 10 to 17) within the NEE phase ($\mu = 1.75$ and $\gamma = 1.6$), obtained by solving numerically the cavity Eq. (12). Both axes are rescaled by the Thouless energy $N^{(1-\gamma)/(\mu-1)}$. We also show the results of exact diagonalizations up to $n = 14$ (empty symbols) which are in good agreement with the cavity calculation except in the regime $\eta \ll 1/N$, as expected, due to the fact that the spectral statistics of finite-size matrices always appears as localized if η is smaller than the mean-level spacing. The grey lines corresponds to the localized behavior $\text{Im}\mathcal{G}_{\text{typ}} \propto \eta$ found for $\eta \ll N^{-1}$ and for $\eta \gg E_{\text{Th}}$. Similar results are found within the whole NEE phase $1 < \mu < 2$ and $1 < \gamma < \mu$.

If η is smaller than the typical value of S_i , then $\text{Im}\mathcal{G}$ becomes independent of η on all sites and its probability distribution is given by Eq. (15) with η replaced by S_i . The $\mu/2$ th moment of $\text{Im}\mathcal{G}$ must then be determined self-consistently from Eqs. (13) and (16), yielding

$$\langle |\text{Im}\mathcal{G}|^{\frac{\mu}{2}} \rangle \propto N^{-\frac{\gamma-1}{\mu-1}} (1-\frac{\mu}{2}),$$

$$[S(z)]_{\text{typ}} \propto N^{-\frac{\gamma-1}{\mu-1}}.$$

If instead η is larger than $[S(z)]_{\text{typ}}$, on most of the sites the regulator dominates over S_i . We thus have that

$$\text{Im}\mathcal{G}_{\text{typ}} \propto \begin{cases} N^{(1-\gamma)/(\mu-1)} & \text{for } \eta \ll N^{(1-\gamma)/(\mu-1)} \\ \eta & \text{for } \eta \gg N^{(1-\gamma)/(\mu-1)}. \end{cases} \quad (17)$$

This behavior is confirmed by Fig. 3, where we plot the typical value of the imaginary part of the Green's function obtained by solving numerically Eq. (12) for several values of the regulator η and for several system sizes $N = 2^n$ (with n from 10 to 17 and averaging the data over 2^{23-n} independent realizations) within the intermediate phase ($\mu = 1.75$ and $\gamma = 1.6$). The figure shows that for N large the curves corresponding to different size approach a limiting curve when the η and the $\text{Im}\mathcal{G}_{\text{typ}}$ axis are rescaled by the Thouless energy $N^{(1-\gamma)/(\mu-1)}$, as predicted by Eq. (17). In particular, the plateau establishing for $\eta \ll E_{\text{Th}}$ is clearly visible, although some finite-size effects are still at play even for the largest system size $N = 2^{17}$. We also show the results of exact diagonalizations up to $N = 2^{14}$ (averaged over 2^{20-n} realizations) which are in very good agreement with the cavity solution, except in the regime $\eta \ll 1/N$. In fact, when the regulator becomes much smaller than the mean-level spacing, finite-size L-RP matrices

again exhibit the localized behavior, $\text{Im}\mathcal{G}_{\text{typ}} \propto N^{D_1} \eta$ [79], as expected.

This analysis reveals the existence of a crossover energy scale $E_{\text{Th}} \simeq [S(z)]_{\text{typ}} \propto N^{(1-\gamma)/(\mu-1)}$ over which $\text{Im}\mathcal{G}_{\text{typ}}$ has a delocalizedlike behavior and is independent of η , in full agreement with the results given in Sec. III. The origin of such a crossover scale is due to the fact that wave functions close in energy are hybridized by the off-diagonal perturbation and form minibands. Within the cavity approach, the effective width of the minibands is self-consistently determined by finding the width of the energy interval such that $|E - \epsilon_i| \lesssim S_i$.

Equation (17) also yields a prediction for the spectral fractal exponent D_1 . In fact, by definition one has that

$$\rho_{\text{typ}} = \frac{e^{\langle \ln \text{Im}\mathcal{G} \rangle}}{\langle \text{Im}\mathcal{G} \rangle} \propto N^{D_1-1}.$$

Since $\langle \text{Im}\mathcal{G} \rangle \sim \pi p(E)$ is of order 1 in the whole intermediate NEE phase (as well as in the AL phase), from the asymptotic behavior of the Green's functions one immediately finds that in the large N limit, D_1 is given by Eq. (6).

There are several important differences with respect to the Gaussian RP model [47,48] due to the fact that the self-energy S_i is broadly distributed (which seems to be common to MBL systems [16,57]):

In the Gaussian RP ensemble, the width of the minibands is simply given by the average effective spectral bandwidth $\Gamma_{\text{av}} = \langle S_i(z) \rangle$ that a particle created in i can reach, Eq. (10): $E_{\text{Th}} \sim N \langle \mathcal{H}_{ij}^2 \rangle \sim N^{1-\gamma}$. As discussed above and illustrated in Fig. 1, for its L-RP counterpart one can in principle define a typical and an average bandwidth which exhibit a different scaling with N for $\mu < 2$:

$$\Gamma_{\text{typ}} \approx 2\pi \rho N [\mathcal{H}_{ij}^2]_{\text{typ}} \sim N^{1-2\gamma/\mu},$$

$$\Gamma_{\text{av}} \approx 2\pi \rho N \langle \mathcal{H}_{ij}^2 \rangle_W \sim N^{1-\gamma}.$$

These energy scales are both different from the Thouless energy, $\Gamma_{\text{typ}} \ll E_{\text{Th}} = N^{(1-\gamma)/(\mu-1)} \ll \Gamma_{\text{av}}$, which is instead determined self-consistently as the typical value of the self-energy which sets the scale at which the spectral statistics exhibits a crossover.

Note that the scaling of Γ_{typ} , Γ_{av} , and E_{Th} all coincide and become equal to the ones of the Gaussian RP ensemble $N^{1-\gamma}$ for $\mu \rightarrow 2$. Therefore, for $\mu \geq 2$, the minibands in the local spectrum become *fractal* (and not multifractal) and the anomalous dimensions become degenerate, $D_q = D$ for $q > 1/2$ [44].

VI. NUMERICAL STUDY OF THE FRACTAL DIMENSIONS

The analytical predictions Eqs. (6) and (7) can be directly checked by the analysis of the finite-size scaling behavior of the flowing fractal dimension $D_1(N, \gamma)$ and $D_\infty(N, \gamma)$, which can be measured either from the full numerical solution of the cavity Eqs. (12) or from exact diagonalizations. Solving Eqs. (12) for $N \times N$ matrices of the L-RP ensemble and averaging the results over many (2^{23-n}) independent realizations of the disorder, one can estimate $D_1(N, \gamma)$ from the derivative

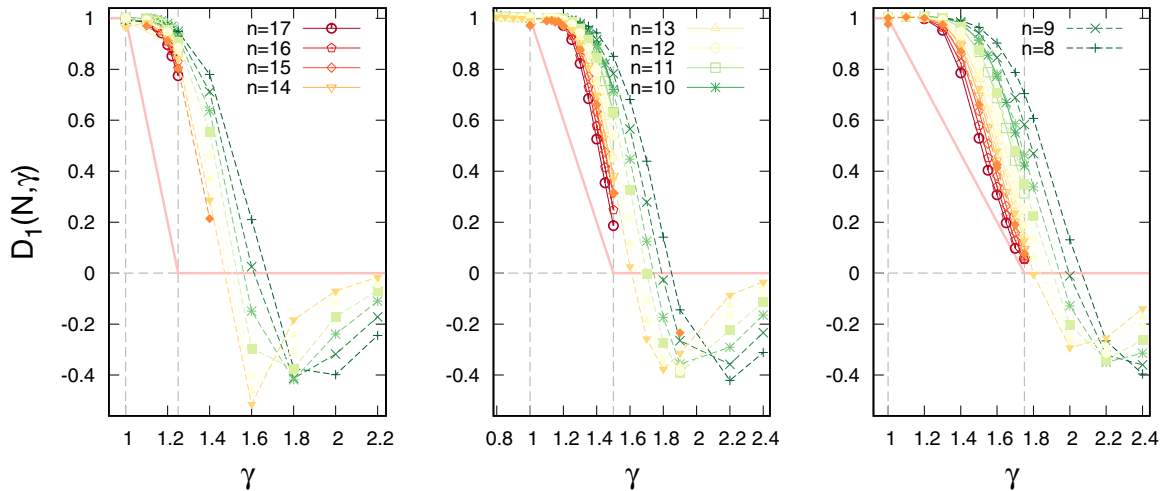


FIG. 4. Flowing N -dependent fractal dimensions $D_1(N, \gamma)$ for $\mu = 1.25$ (left), $\mu = 1.5$ (middle), $\mu = 1.75$ (right), and $N = 2^n$ with $n = 8, \dots, 17$. The pink lines correspond to the analytic prediction Eq. (6). $D_1(N, \gamma)$ is computed either from the numerical solution of the cavity Eqs. (12) and using Eq. (18) (continuous curves, for $10 \leq n \leq 17$), or via Eq. (19) from the scaling of the first moment of the wave functions' amplitudes measured from exact diagonalizations (dashed curves, for $8 \leq n \leq 15$). The results obtained using these two procedures are essentially indistinguishable within the numerical accuracy for all values of N , μ , and γ considered.

of the logarithm of $\rho_{\text{typ}}(N, \gamma)$ with respect to $\ln N$:

$$D_1(N, \gamma) = 1 + \frac{\partial \ln \rho_{\text{typ}}(N, \gamma)}{\partial \ln N}. \quad (18)$$

(Hereafter the logarithmic derivatives are computed as discrete derivatives involving the three available values of the system size closest to N .) Similarly, $D_1(N, \gamma)$ can be also computed via exact diagonalizations from the scaling behavior of the first moment of the wave-function amplitudes with the system size:

$$\Upsilon_1(n) = - \sum_{i=1}^N |\psi_n(i)|^2 \ln(|\psi_n(i)|^2), \quad (19)$$

$$D_1(N, \gamma) = \frac{\partial \ln(\Upsilon_1(N, \gamma))}{\partial \ln N}.$$

($\langle \Upsilon_1(N, \gamma) \rangle$) is averaged over 2^{20-n} samples and over eigenvectors within a given energy band around the middle of the spectrum, $E_n \in [-W/4, W/4]$.) The numerical results obtained using these two procedures are shown in Fig. 4 as a function of γ for three values of μ and for several values of the system size. The figure illustrates that the estimations for $D_1(N, \gamma)$ obtained from the cavity approach and from exact diagonalizations are essentially indistinguishable within the numerical uncertainties (see also Fig. 11), which is not surprising since the cavity equations are asymptotically exact for the L-RP ensemble at large N . The quasiplateau of $D_1(N, \gamma)$ observed close to the ergodic transition, $\gamma \gtrsim 1$, is a manifestation of the fact that the line of critical points separating the delocalized regime from the NEE one is in the ergodic phase.

From exact diagonalizations, one can also measure higher moments of the wave-function amplitudes:

$$\Upsilon_q(n) = \ln \left(\sum_{i=1}^N |\psi_n(i)|^{2q} \right), \quad (20)$$

$$(q-1)D_q(N, \gamma) = - \frac{\partial \ln(\Upsilon_q(N, \gamma))}{\partial \ln N}.$$

The flowing fractal exponent $D_2(N, \gamma)$, associated with the scaling with N of the inverse participation ratio (IPR) is plotted in Fig. 13 of Appendix D, showing that $D_2(N, \gamma)$ has the same qualitative behavior of (and is slightly smaller than) $D_1(N, \gamma)$. In the left panel of Fig. 5, we plot $D_q(N, \gamma)$ for $q = 1$ (red), $q = 6$ (green), and $q \rightarrow \infty$ (blue) for $\mu = 1.75$ within the NEE phase, showing that $D_\infty < D_6 < D_1$.

To check that the $D_1(N, \gamma)$ and $D_\infty(N, \gamma)$ asymptotically approach the theoretical predictions in the large N limit, we have performed a finite-size scaling analysis of the distance between the flowing fractal exponents from their theoretical asymptotic value, Eqs. (6) and (7). To have that the data at different values of N and γ vary on the same scale (i.e., between 0 and 1), we have considered the ratio of $D_1(N, \gamma) - D_1(\gamma)$ [respectively, $D_\infty(N, \gamma) - D_\infty(\gamma)$] divided by the amplitude of the same quantity at small N , $D_1(N, \gamma = 1) - D_1(\gamma)$ [resp. $D_\infty(N, \gamma = 1) - D_\infty(\gamma)$] [11,36]. The middle and right panels of Fig. 5 clearly show that a very good collapse is obtained for all values of μ when the data for $q = 1$ and $q = \infty$ are plotted in terms of the scaling variable $(\gamma - \gamma_{\text{ergo}})(\ln N)^{1/\nu_{\text{ergo}}}$, with $\gamma_{\text{ergo}} = 1$. The best collapse is found for $\nu_{\text{ergo}} = 1$ independently of μ (see Fig. 7), as for the RP model [50]. This finite-size scaling analysis confirms that the fractal dimensions are not degenerate for $\mu < 2$, as anticipated above as a direct consequence of the multifractality of the minibands.

As shown in Figs. 14 and 15 of Appendix D, an independent estimation of ν_{ergo} can also be obtained by performing

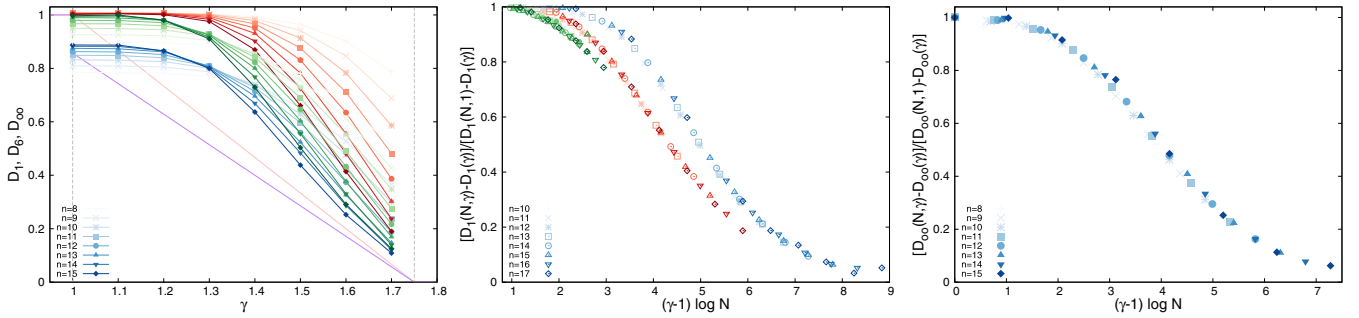


FIG. 5. The left panel shows the flowing N -dependent fractal dimensions $D_1(N, \gamma)$ (red), $D_6(N, \gamma)$ (green), and $D_\infty(N, \gamma)$ (blue) for $\mu = 1.75$ in the NEE phase ($1 < \gamma < \mu$) for $N = 2^n$ with $n = 8, \dots, 15$. The fractal dimensions are estimated via Eqs. (19) and (20). The pink line corresponds to the analytic prediction for D_1 , Eq. (6), while the violet line shows the analytic prediction for D_∞ , Eq. (7). The middle and right panels show the finite-size scaling analysis of the distance of the flowing N -dependent fractal dimensions $D_1(N, \gamma)$ and $D_\infty(N, \gamma)$ from their theoretical asymptotic values, Eqs. (6) and (7), divided by the same quantities at small N , for $\mu = 1.25$ (green), $\mu = 1.5$ (red), $\mu = 1.75$ (blue). A very good data collapse is obtained for all values of μ when the ratios $[D_1(N, \gamma) - D_1(\gamma)]/[D_1(N, 1) - D_1(\gamma)]$ and $[D_\infty(N, \gamma) - D_\infty(\gamma)]/[D_\infty(N, 1) - D_\infty(\gamma)]$ are plotted as a function of the scaling variable $(\gamma - 1) \ln N$.

a finite-size scaling analysis of the moments of the wavefunction amplitudes with the system size similar to the one proposed in Refs. [11] (and inspired by the analysis of Ref. [36]) on the insulating side of the MBL transition. This analysis confirms that $\nu_{\text{ergo}} = 1$ at the ergodic transition independently of μ .

VII. LEVEL STATISTICS

In this section, we show finite-size scaling analysis of the level statistics obtained from exact diagonalizations of L-RP random matrices of size $N = 2^n$ with n ranging from 8 to 15. Averages are performed over 2^{20-n} different realizations of the disorder and over eigenstates within an energy window around the middle of the spectrum, $E_n \in [-W/4, W/4]$.

We start by focusing on the level statistics of neighboring eigenvalues and measure the ratio of adjacent gaps:

$$r_n = \min \left\{ \frac{E_{n+2} - E_{n+1}}{E_{n+1} - E_n}, \frac{E_{n+1} - E_n}{E_{n+2} - E_{n+1}} \right\},$$

whose probability distribution displays a universal form depending on the level statistics, with $\langle r \rangle$ equal to 0.53 in the GOE ensemble and to 0.39 for Poisson statistics [80].

The transition from GOE to Poisson statistics can also be captured by correlations between adjacent eigenstates such as the mutual overlap between two subsequent eigenvectors, defined as

$$q_n = \sum_{i=1}^N |\psi_n(i)| |\psi_{n+1}(i)|,$$

In the GOE phase, $\langle q \rangle$ converges to $2/\pi$ (as expected for random vector on a N -dimensional sphere), while in the localized phase two successive eigenvector are typically peaked around different sites and do not overlap and $\langle q \rangle \rightarrow 0$.

In the left and middle panels of Fig. 6, we plot $\langle r \rangle$ (top) and $\langle q \rangle$ (bottom) as a function of γ for $\mu = 1.25$ and $\mu = 1.5$, showing that both observables take their GOE universal values for $\gamma \leq \mu$ and seem to approach the Poisson universal values for $\gamma > \mu$ in the thermodynamic limit. The right panels demonstrate that a very good collapse is obtained for both observables and for all values of $\mu \in (1, 2)$ when the data are plotted in terms of the scaling variable $(\gamma - \gamma_{\text{AL}})(\ln N)^{1/\nu_{\text{AL}}}$ (with $\gamma_{\text{AL}} = \mu$), confirming that the level statistics of neighboring gaps exhibit a transition from GOE to Poisson at the AL transition. Hence, similarly to the Gaussian RP and LN-RP models, the level statistics is locally Wigner-Dyson

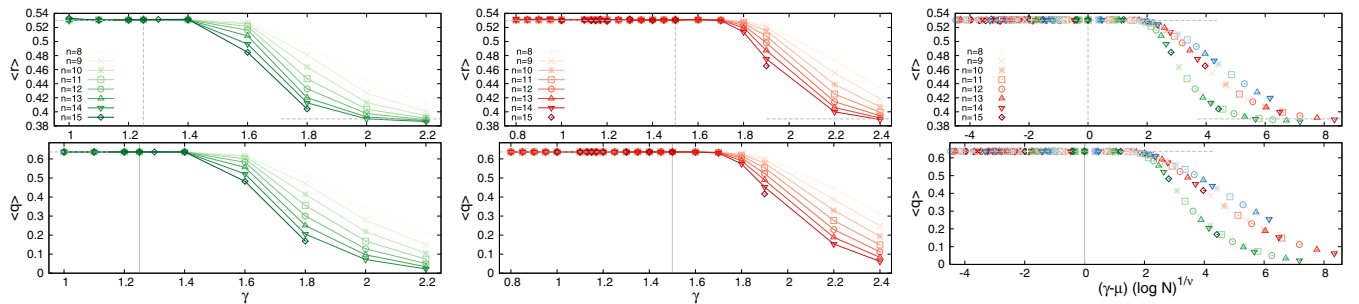


FIG. 6. $\langle r \rangle$ (top) and $\langle q \rangle$ (bottom) as a function of γ for $\mu = 1.25$ (left panels), $\mu = 1.5$ (middle panels) for several system sizes $N = 2^n$ with n from 8 to 15 (different values of n correspond to different symbols as indicated in the legend). The right panels show that a very good data collapse is obtained for both $\langle r \rangle$ and $\langle q \rangle$ for all values of $\mu \in (1, 2)$ in terms of the scaling variable $(\gamma - \gamma_{\text{AL}})(\ln N)^{1/\nu_{\text{AL}}}$, with $\gamma_{\text{AL}} = \mu$ and $\nu_{\text{AL}}^{-1} \approx 0.99$ for $\mu = 1.75$ (blue), $\nu_{\text{AL}}^{-1} \approx 0.98$ for $\mu = 1.5$ (red), and $\nu_{\text{AL}}^{-1} \approx 0.9$ for $\mu = 1.25$ (green). The horizontal dashed grey lines correspond to the GOE and Poisson universal values.

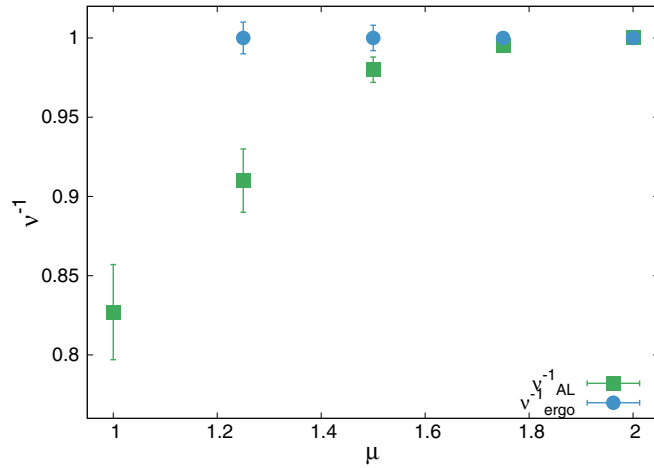


FIG. 7. Critical exponents ν_{AL} and ν_{ergo} yielding the best data collapse for the level statistics at the Anderson localization transition (see Figs. 6 and 8) and for the fractal dimensions at the ergodicity breaking transition (see Fig. 5).

in the whole NEE phase since the eigenvectors within the same miniband strongly overlap. As anticipated in Sec. IV, the critical point is in the GOE phase for all values of μ , as indicated by the fact that $\langle r \rangle$ and $\langle q \rangle$ take their GOE universal values for $\gamma_{\text{AL}} = \mu$. The exponent ν_{AL} that produces the best collapse is found to decrease continuously as μ is increased and approaches the RP value $\nu_{\text{AL}}^{-1} = 1$ for $\mu = 2$ [50] (see Fig. 7).

For $\mu = 1$, a reasonably good data collapse of the observables $\langle r \rangle$ and $\langle q \rangle$ related to the statistics of neighboring gaps cannot be achieved by using $(\gamma - 1)(\ln N)^{1/\nu_{\text{AL}}}$ as a scaling variable for any value of ν_{AL} , and we have therefore attempted a different finite-size scaling analysis, as illustrated in Fig. 8. More specifically, we plot the distance of $\langle r \rangle(\gamma, N)$ and $\langle q \rangle(\gamma, N)$ from their values at the critical point ($\langle r \rangle_c \approx 0.53$ and $\langle q \rangle_c = 2/\pi$ for $\gamma = 1$) as a function of the

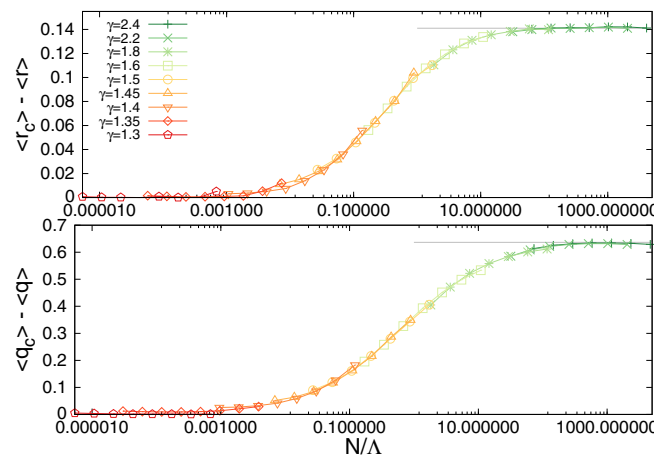


FIG. 8. $\langle r \rangle(1, N) - \langle r \rangle(\gamma, N)$ (top) and $\langle q \rangle(1, N) - \langle q \rangle(\gamma, N)$ (bottom) as a function of the scaling variable $N/\Lambda(\gamma)$. A good data collapse for both observables is obtained for $\Lambda(\gamma) \sim \exp[A(\gamma - 1)^{-\nu_{\text{AL}}}]$, with $\nu_{\text{AL}} \approx 1.2$. The horizontal dashed grey lines represent the difference between the GOE and Poisson asymptotic values.

scaling variable $N/\Lambda(\gamma)$, where $\Lambda(\gamma)$ is a correlation volume that depends on the distance from the critical point. A very good data collapse of both $\langle r \rangle$ and $\langle q \rangle$ is obtained for $\Lambda \sim \exp[A(\gamma - 1)^{-\nu_{\text{AL}}}]$ with $\nu_{\text{AL}} \approx 1.2$. Such volumic scaling is similar to the critical scaling observed on the delocalized side of the Anderson model on the Bethe lattice [36] and reflects the fact that at the tricritical point ($\mu = 1$, $\gamma = 1$) the fractal dimension exhibits a discontinuous jump from $D_1 = 1$ for $\gamma = 1$ to $D_1 \rightarrow 0$ for $\gamma \rightarrow 1^+$. However, in the present case the situation is somehow reversed compared to the Anderson model on the Bethe lattice, in the sense that here the critical point is in the delocalized phase (i.e., $D_1 = 1$ for $\mu = 1$ and the level statistics is GOE) and the scaling in terms of an exponentially large correlation volume is found on the *localized* side of the transition, while for the Anderson model on the Bethe lattice the critical point is in the localized phase (i.e., $D = 0$ at W_c and the statistics is Poisson) and the volumic scaling is found on the *delocalized* side of the transition [36,38,75].

VIII. OVERLAP CORRELATION FUNCTION

It is also worthwhile to study the behavior of the spectral correlation function $K_2(\omega)$ between eigenstates at different energies, which provides a very useful probe of the level statistics and on the statistics of wave-functions' amplitudes, and allows one to distinguish between ergodic, localized, and multifractal states [81–84]:

$$K_2(\omega) = \left\langle \sum_i |\psi_n(i)\psi_m(i)|^2 \delta(E_n - E_m - \omega) \right\rangle \quad (21)$$

$$\simeq \lim_{\eta \rightarrow 0^+} \left\langle \frac{N \sum_i \text{Im} \mathcal{G}_{ii}(\omega/2) \text{Im} \mathcal{G}_{ii}(-\omega/2)}{\sum_i \text{Im} \mathcal{G}_{ii}(\omega/2) \sum_i \text{Im} \mathcal{G}_{ii}(-\omega/2)} \right\rangle.$$

Furthermore, $K_2(\omega)$ is the Fourier transform of the return probability and can be thought of as proxy for the correlation function of local operators, e.g., the spin-spin correlation function, in the problem of MBL [19,85–87].

For GOE matrices, $K_2(\omega) = 1$ identically, independently on ω on the entire spectral bandwidth. In the standard (ergodic) metallic phase (i.e., the weakly ergodic phase using the terminology of Ref. [59]), $K_2(\omega)$ has a plateau at small energies, for $\omega < E_{\text{Th}}$, followed by a fast decay which is described by a power law, with a system-dependent exponent [82]. The height of the plateau is larger than one, which implies an enhancement of correlations compared to the case of independently fluctuating Gaussian wave functions. The Thouless energy which separates the plateau from the power-law decay stays finite in the thermodynamic limit and extends to larger energies as one goes deeply into the metallic phase, and corresponds to the energy band over which GOE-like correlations establish [81].

The behavior of the overlap correlation function for multifractal wave functions is instead drastically different: In the NEE phase of the Gaussian RP ensemble, for instance, the plateau is present only in a narrow energy interval, as E_{Th} shrinks to zero in the thermodynamic limit (still staying much larger than the mean level spacing), while its height grows as N^{1-D_2} . Beyond E_{Th} , eigenfunctions poorly overlap with each

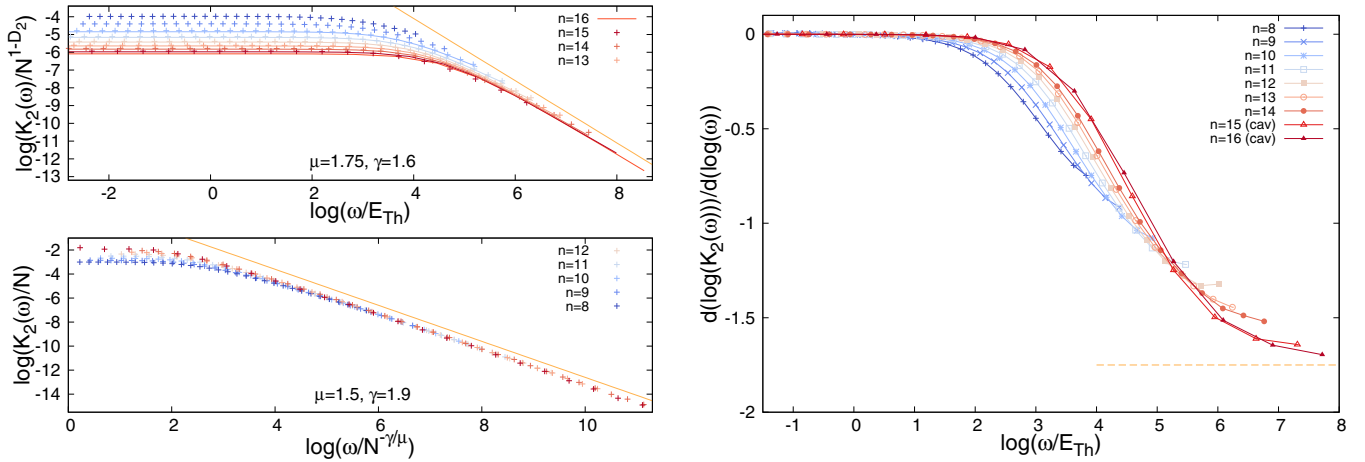


FIG. 9. Top left: Logarithm of the overlap correlation function versus $\ln \omega$ in the NEE phase, $\mu = 1.75$ and $\gamma = 1.6$, for several system sizes $N = 2^n$, with $n = 8, \dots, 16$ (different colors correspond to different values of n). The results obtained from exact diagonalizations (for $8 \leq n \leq 15$) are represented with points, while the results obtained using the cavity approach (for $10 \leq n \leq 16$) are represented with full lines. The energy axis is rescaled by the Thouless energy $E_{\text{Th}} = N^{(1-\gamma)/(\mu-1)}$, while the vertical axis is rescaled by N^{1-D_2} (with $D_2 \approx 0.19 \lesssim D_1 = 0.2$), i.e., the value of $K_2(\omega)$ for $\omega \rightarrow 0$. Bottom left: Logarithm of the overlap correlation function as a function of $\ln \omega$ in the AL phase, $\mu = 1.5$ and $\gamma = 1.9$, for several system sizes. The energy axis is rescaled by $N^{-\gamma/\mu}$, while the vertical axis is rescaled by N . The plateau at small energy is followed in both phases by a power-law decay $K_2(\omega) \propto 1/\omega^\mu$ (orange lines). Right: Derivative $\partial \ln K_2(\omega)/\partial \ln \omega$ as a function of $\ln(\omega/E_{\text{Th}})$ for $\mu = 1.75$, $\gamma = 1.6$, and for several system sizes $N = 2^n$, which gives a running with ω and N exponent θ of a local power-law describing the decay of $K_2(\omega)$. $\theta = 0$ for $\omega < E_{\text{Th}}$ (as in the Gaussian RP and in LN-RP models), while for $\omega \gg E_{\text{Th}}$ the exponent θ tends to μ at large N , corresponding to a nontrivial fractal structure of the set of minibands. Data for $8 \leq n \leq 14$ have been obtained from exact diagonalizations while data for $n = 15, 16$ have been obtained using the cavity approach.

other and the statistics is no longer GOE and $K_2(\omega)$ decay to zero as a power law, $K_2(\omega) \sim (\omega/E_{\text{Th}})^{-2}$ [44].

Our numerical results are presented in Fig. 9. The overlap correlation function is computed using both exact diagonalizations (averages are performed over 2^{20-n} different realizations of the disorder and over eigenstates within an energy window around the middle of the spectrum, $E_n \in [-W/4, W/4]$) and its spectral representation in terms of the Green's functions obtained via the cavity method [88] (averaging over 2^{23-n} samples), finding a very good agreement between the two approaches. In the top panel, we plot $K_2(\omega)$ for several system sizes in the NEE phase, $\mu = 1.75$ and $\gamma = 1.6$, and we show that in the large N limit the data corresponding to different sizes approach a limiting curve when the energy is rescaled by the Thouless energy $E_{\text{Th}} = N^{(1-\gamma)/(\mu-1)}$ and the vertical axis is rescaled by N^{1-D_2} , where $D_2 \lesssim D_1$. (A similar behavior is observed for other values of μ and γ within the multifractal phase.) The fact that $K_2(\omega)$ is constant for $N^{-1} < \omega < E_{\text{Th}}$ reflects the fact that the minibands are locally compact, as in the Gaussian RP model (i.e., the fractal dimension of the local spectrum *inside* a mini-band is equal to 1). At larger energy separation, $\omega \gg E_{\text{Th}}$, the exponent $\theta = -\partial \ln K_2(\omega)/\partial \ln \omega$ reflects instead the fractal structure of the set of mini-bands [59]. For the Gaussian RP $\theta = 2$ [44,47,49], while, as shown in the right panel of Fig. 9, θ tends to μ at large N in the NEE regime, $\mu \in (1, 2)$ and $\gamma \in (1, \mu)$, irrespectively of the value of γ . This suggests that the minibands in the local spectrum of the L-RP ensemble are constituted by a compact set of subsequent levels ($\Delta_{\text{typ}} \sim \langle \Delta \rangle \sim N^{-1}$, as in the Gaussian RP case) whose envelope follows the power-law decay of the LDoS profile.

In the bottom panel of Fig. 9, we show the results in the AL phase, $\mu = 1.5$ and $\gamma = 1.9$. In this case, $K_2(\omega)$ displays the usual localized behavior, despite the fact that for $\gamma < 2$ the average effective bandwidth $\Gamma_{\text{av}} \sim N \langle \mathcal{H}_{ij}^2 \rangle_W \sim N^{1-\gamma}$ is still much larger than the mean-level spacing N^{-1} . A good collapse of the data at different N is obtained when the vertical axis is rescaled by N ($D_2 = 0$) and the energy axis is rescaled by $N^{-\gamma/\mu}$. The plateau that extends up to an energy scale $N^{-\gamma/\mu} < N^{-1}$ corresponds to rare resonances when $\omega < |\mathcal{H}_{ij}|_{\text{typ}}$. Also in the AL regime, the plateau at small energy is followed by a fast decrease $K_2(\omega) \propto 1/\omega^\mu$ (orange line).

IX. CONCLUSIONS

In this paper, we have studied a generalization of the RP ensemble when the off-diagonal perturbation belongs to the Lévy universality class [53], with i.i.d. matrix elements with power-law tails of exponent $1 + \mu$ and typical value scaling as $N^{-\gamma/\mu}$. We believe that the L-RP ensemble provides a more realistic benchmark to develop an effective description of delocalization of the wave functions in interacting many-body disordered systems, in which the effective transition rates between distant states in the Hilbert space correspond to a long series of quantum transitions and are in general broadly distributed [13,16,23,57].

The most important feature of the model is that, due to the fat tails of the off-diagonal matrix elements, sites at energy separation much larger than the typical bandwidth $N[\mathcal{H}_{ij}^2]_{\text{typ}}$ can be hybridized by anomalously large rare matrix elements, producing a NEE phase with multifractal minibands. In this sense, the L-RP ensemble is much richer than its Gaussian

RP counterpart, since the minibands in the local spectrum are multifractal and the spectrum of fractal dimension is not degenerate.

One of the most important outcomes of our analysis is the formulation of a simple, intuitive, and physically transparent argument that allows one to characterize the multifractal structure of the minibands and determine the fractal dimensions of the eigenstates in the NEE phase, as well as the phase diagram of the system. The basic idea is that the Thouless energy can be determined self-consistently by imposing that hybridization occurs provided that the largest matrix elements between a site i and the other N^{D_1} sites j within a given miniband are of the same order of the energy spreading of the miniband itself. This argument is very general and can in principle be extended and adapted to analyze the multifractal states also in more complex situations in which, for instance, the effective transition rates are correlated [60] and/or depend on the positions i and j in the reference space and on the energy separation $|\epsilon_i - \epsilon_j|$, as in many-body problems [13,16,23,57]. Extending our analysis to these situations is certainly a promising direction for future investigations.

The predictions of such simple arguments are fully confirmed both analytically, by a thorough analysis of the self-consistent equations for the diagonal elements of the resolvent matrix obtained using the cavity approach, and numerically, by means of extensive exact diagonalizations, and are also in full agreement with the rule of thumb criteria for localization and ergodicity recently put forward in Refs. [48,58–60].

Another interesting feature of the model is the existence of a tricritical point [58,59] for $\mu = 1$ (i.e., Cauchy distributed off-diagonal elements [70]) and $\gamma = 1$, where the fractal dimensions exhibit a discontinuous jump from $D_1 = 1$ for $\gamma = 1$ to $D_1 \rightarrow 0$ for $\gamma \rightarrow 1^+$. This is somehow a specular behavior compared to the Anderson model on the Bethe lattice: Here the tricritical point is in the delocalized phase (i.e., $D_1 = 1$ for $\mu = 1$ and the level statistics is GOE) and the scaling in terms of an exponentially large correlation volume is found on the *localized* side of the transition, while for the Anderson model on the Bethe lattice the critical point is in the localized phase (i.e., $D = 0$ at W_c and the statistics is Poisson) and the volume scaling is found on the *delocalized* side of the transition [36,38,75].

ACKNOWLEDGMENTS

We would like to warmly thank I. M. Khaymovich and V. E. Kravtsov for many enlightening and helpful discussions. This work was partially supported by a grant from the Simons Foundation (Grant No. 454935, G.B.).

APPENDIX A: $\mu \in (0, 1)$

As discussed in Sec. III, for $\mu < 1$ the Lévy-RP ensemble exhibits a single discontinuous transition at $\gamma = 1$ between a phase for $\gamma > 1$ in which the off-diagonal Lévy matrix elements are a small regular perturbation and \mathcal{H} is close to \mathcal{A} (and eigenvectors are fully localized) to a phase for $\gamma < 1$ in which the off-diagonal matrix elements dominate and \mathcal{H} is close to \mathcal{L} . This is confirmed by the numerical results (not

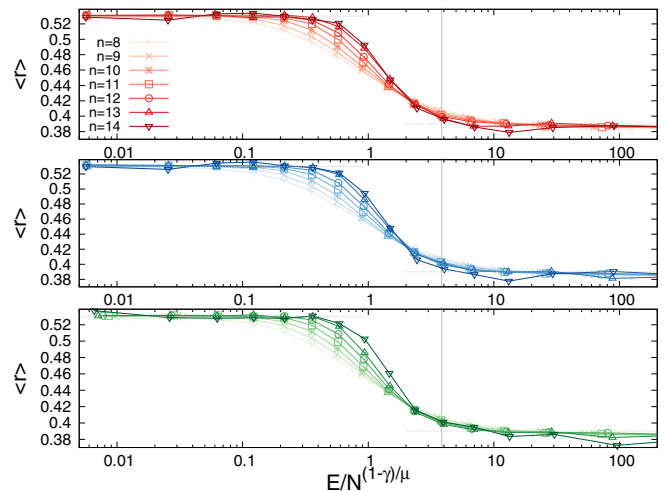


FIG. 10. $\langle r \rangle$ as a function of the energy (rescaled by $N^{(\gamma-1)/\mu}$ to have an N -independent spectrum in the thermodynamic limit) for $\mu = 0.5$, for several system sizes $N = 2^n$ with n from 8 to 14 (different values of n correspond to different symbols as indicated in the legend) and for $\gamma = 0$ (top, red), $\gamma = 0.4$ (middle, blue), and $\gamma = 0.8$ (bottom, green). The data indicated the presence of a transition from GOE statistics to Poisson statistics when the energy is increased above E_{loc} , as already studied in Ref. [62]. There is no notable difference between the curves at different values of γ within the numerical accuracy, implying that the AL transition is not affected by the scaling of the diagonal energies. The vertical grey lines show the position of the mobility edge $E_{loc} \approx 3.85$ computed analytically in Ref. [62] for $W = 0$, while the horizontal dashed grey lines correspond to the GOE and Poisson asymptotic values.

shown) that indeed clearly indicate that the level statistics tends to Poisson for $\gamma > 1$. However, from the analysis of Ref. [62], one knows that Lévy matrices have a mobility edge which separates an extended phase at low energy from a AL phase at high energy. For the natural scaling $\gamma = 1$, when the typical value of \mathcal{L}_{ij} is of order $N^{-1/\mu}$ (and the eigenvalues of \mathcal{L} are of order 1), the mobility edge is found at a finite energy $E_{loc}(\mu)$ (which can be computed analytically [62]). $E_{loc}(\mu)$ goes to 0 for $\mu \rightarrow 0$ and to $+\infty$ for $\mu \rightarrow 1^-$. In other words, the fraction of extended and localized eigenstates of the spectrum are both extensive for $\mu \in (0, 1)$; the fraction of extended states vanishes for $\mu \rightarrow 0$ while the fraction of localized states vanishes for $\mu \rightarrow 1^-$. When $\gamma < 1$, the eigenvalues of \mathcal{L} are all rescaled by $N^{(1-\gamma)/\mu}$ and the mobility edge is thus found at energy $E_{loc}(\mu)N^{(1-\gamma)/\mu}$. We then expect that the phase transition taking place at $\gamma = 1$ is in fact split in two: At low energy, $E < E_{loc}(\mu)N^{(1-\gamma)/\mu}$, one has a discontinuous phase transition from the extended phase of Lévy matrices for $\gamma < 1$ to a AL phase dominated by the diagonal disorder for $\gamma > 1$; At high energy, $E > E_{loc}(\mu)N^{(1-\gamma)/\mu}$, instead, one has a discontinuous transition from two different localized phases, namely, a phase for $\gamma < 1$ where eigenstates are close to the AL eigenstates of the off-diagonal Lévy matrix, to a phase for $\gamma > 1$ in which the eigenstates are localized due to the diagonal disorder.

This scenario is fully confirmed by the numerical results of Fig. 10, where we plot $\langle r \rangle$ as a function of the energy (rescaled by $N^{(\gamma-1)/\mu}$ in order to have energies of order 1) for $\mu = 0.5$,

for several system sizes, and for three values of γ (the data are averaged over 2^{20-n} independent realizations). The curves indicate the presence of a transition from GOE statistics to Poisson statistics when the energy is increased above E_{loc} , as already studied in Ref. [62]. In the rescaled variables, such transition does not show any notable dependence on γ .

APPENDIX B: STABILITY OF NON-ERGODIC STATES AGAINST HYBRIDIZATION

In this Appendix, we discuss the stability criterion of non-ergodic states against hybridization put forward in Ref. [59] for the LN-RP ensemble. Let us consider two states ψ_n and ψ_m on different fractal support sets. Let us assume that both states are multifractal and occupy N^{D_1} sites of a support set where $|\psi(i)|^2 \sim N^{-D_1}$.

We now apply the usual Mott's argument for hybridization of states when the disorder realization changes from \mathcal{L}_{ij} to \mathcal{L}'_{ij} . The new idea of Ref. [59] is to compute the hopping matrix element \mathcal{V}_{nm} between the states and not between the sites as is customary,

$$\mathcal{V}_{nm} = \sum_{i,j} \delta \mathcal{L}_{ij} \psi_n(i) \psi_m(j),$$

where $\psi_n(i)$ is the eigenfunction of the n th state of \mathcal{H} . $\delta \mathcal{L}_{ij} = \mathcal{L}_{ij} - \mathcal{L}'_{ij}$, where \mathcal{L}'_{ij} is drawn from the same Lévy distribution as \mathcal{L}_{ij} and are Lévy distributed random variables with power-law tails of exponent $1 + \mu$ and typical value $2^{1/\mu} N^{-\gamma/\mu}$. For $\mu < 2$, we can thus use the generalized central limit theorem for the sum of heavy-tailed distributed random variables from which we get that \mathcal{V}_{nm} are also Lévy distributed with power-law tails with exponent $1 + \mu$ and typical value:

$$[\mathcal{V}_{nm}]_{\text{typ}} = \left[\frac{2}{N^\gamma} \sum_{i,j} |\psi_n(i)|^\mu |\psi_m(j)|^\mu \right]^{1/\mu}.$$

The moments of the wave functions' amplitudes give by definition $N \langle |\psi_n(i)|^\mu \rangle \sim N^{-D_{\mu/2}(\mu/2-1)}$. Assuming that wave functions belonging to different minibands are not correlated, we have that

$$[\mathcal{V}_{nm}]_{\text{typ}} \sim N^{-\frac{\gamma}{\mu} + D_{\mu/2}(\frac{\mu}{2}-1)}.$$

The condition of stability of the multifractal phase against hybridization is derived similar to the Anderson criteria of stability, Eq. (8), of the localized states. The difference is that now we have to replace the matrix element between the resonant sites \mathcal{L}_{ij} by the matrix element \mathcal{V}_{nm} between the resonant nonergodic states and take into account that on each of $N_S = N^{1-D_1}$ different support sets there are N^{D_1} wave functions which belong to the same miniband and thus are already in resonance with each other. Therefore, the total number of independent-state candidates N_H for hybridization with a given state should be smaller than the total number of states $N_S N^{D_1} = N$ and larger than the number of support sets $N_S = N^{1-D_1}$. In full generality, we posit below that $N_H \propto N^{1-\zeta D_1}$, with $0 < \zeta < 1$. In Ref. [59], the authors chose to use the geometric mean $N_H \propto \sqrt{N N_S} = N^{1-D_1/2}$, i.e., $\zeta = 1/2$. For $1 < \mu < 2$, the Mott's criterion of stability of the multifractal

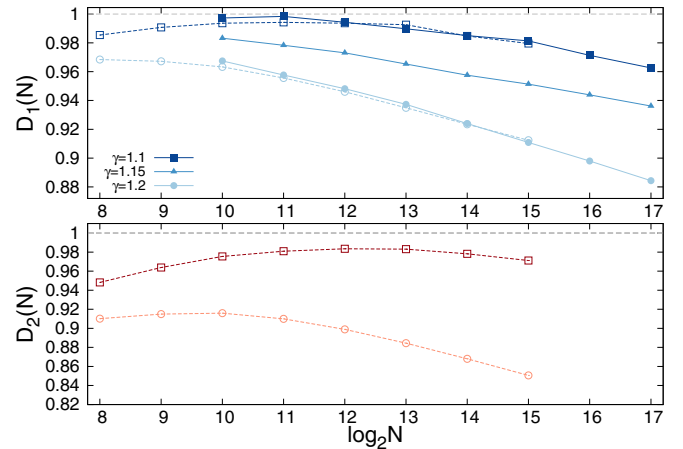


FIG. 11. Flowing N -dependent fractal dimensions $D_1(N, \gamma)$ (top) and $D_2(N, \gamma)$ (bottom) as a function of $\log_2 N$ computed either from the numerical solution of the cavity equations and using Eq. (18) (continuous curves and filled symbols, for $10 \leq n \leq 17$), or via Eqs. (19) and (20) from the scaling of the first and second moments of the wave-function amplitudes measured from exact diagonalizations (dashed curves and empty symbols, for $8 \leq n \leq 15$). The value of $\mu = 1.25$ is chosen in the middle of the region in which the bound Eq. (B1) with $\zeta = 1/2$ would predict that the NEE phase is unstable against hybridization, while the numerical data clearly shows that the anomalous dimensions are smaller than 1 in the large N limit.

phase in the limit $N \rightarrow \infty$ reads

$$N^{1-\zeta D_1} \int_0^W \mathcal{V} P(\mathcal{V}) d\mathcal{V} \sim N^{1-\zeta D_1 - \frac{\gamma}{\mu} + D_{\mu/2}(\frac{\mu}{2}-1)} < \infty.$$

For the RP model, the fractal dimensions are degenerate for $q > 1/2$ [44].

This is not the case for the L-RP ensemble, due to the fact that the minibands are multifractal, as clearly illustrated by Fig. 5. Yet, since D_q is a decreasing function of q , for $1 < \mu < 2$ one can assume that $D_{\mu/2}$ is well approximated by D_1 . This results in an upper bound for the stability of the multifractal phase of the form

$$D_1 \left(\zeta + 1 - \frac{2}{\mu} \right) \geq 1 - \frac{\gamma}{\mu}. \quad (\text{B1})$$

Of course, this condition cannot be fulfilled if $\zeta < 2/\mu - 1$ since the left-hand side becomes negative. This implies that if one chooses $\zeta = 1/2$ as in Ref. [59], one would conclude that the NEE phase is unstable against hybridization in the interval $\mu \in (1, 4/3)$ at least. In fact, plugging the expression Eq. (6) for D_1 into Eq. (B1) one finds that for $\zeta = 1/2$ the stability criterion is never satisfied except at the RP limit $\mu = 2$. Yet this is in strong disagreement with the numerical results on the flowing fractal exponents discussed in the previous section (see Figs. 4 and 5), as further illustrated in Fig. 11 for $\mu = 1.25$, deep in the region where the instability should supposedly take place. This plot shows that $D_1(N, \gamma)$ and $D_2(N, \gamma)$ have a nonmonotonic behavior as a function of N on a characteristic scale that increases as γ is decreased, indicating that in the $N \rightarrow \infty$ limit D_1 and D_2 approach a value

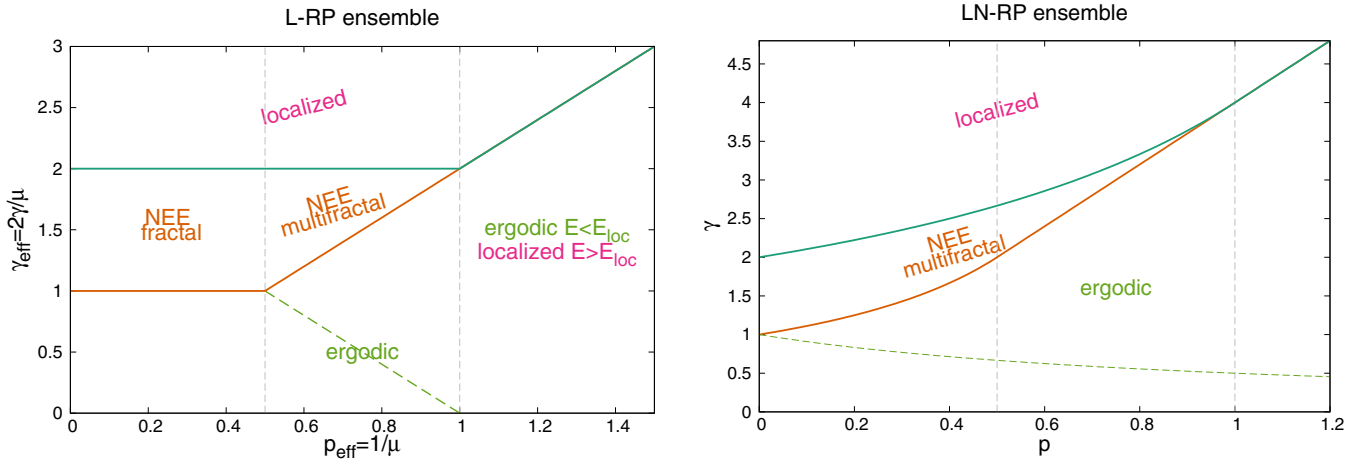


FIG. 12. Left: Phase diagram of the L-RP ensemble of Fig. 2 in the coordinates $\gamma_{\text{eff}} = 2\gamma/\mu$ and $p_{\text{eff}} = 1/\mu$ [89], showing the transitions to the AL phase and to the NEE phase, Eqs. (C2). Right: Phase diagram of the LN-RP ensemble studied in Refs. [58,59], showing the transition lines given in Eqs. (C4) and (C5).

strictly smaller than 1, as expected for a genuine multifractal phase.

A possible way out from this issue is obtained by positing that ζ depends on μ in such a way that the instability is avoided. In fact, assuming that $\zeta > 2/\mu - 1$ and using Eq. (6), one obtains that the stability criterion Eq. (B1) can be fulfilled in the whole NEE phase provided that $\zeta > 1/\mu$. Moreover, for $\zeta = 1/\mu$ the bound Eq. (B1) is saturated, as suggested in Ref. [59].

APPENDIX C: COMPARISON WITH THE LN-RP ENSEMBLE

The model considered in this paper is tightly related to the LN-RP model recently introduced and studied in Refs. [58,59]. In both cases, the off-diagonal matrix elements are broadly distributed, although the specific form of the distribution is slightly different: In particular, the LN-RP model is a modification of the RP random matrix ensemble [44] in which the i.i.d. off-diagonal elements are taken from a log-normal law:

$$P(|\mathcal{H}_{ij}|) = \frac{\exp\left[-\frac{\ln^2(N^{\gamma/2}|\mathcal{H}_{ij}|)}{p\gamma \ln N}\right]}{\sqrt{\pi p\gamma \ln N} |\mathcal{H}_{ij}|}. \quad (\text{C1})$$

The standard RP ensemble is recovered for $p \rightarrow 0$. Note that the effective parameter controlling the scaling of the typical off-diagonal matrix element is introduced similarly to the Gaussian case, $\mathcal{H}_{\text{typ}} \sim N^{-\gamma/2}$, while in the L-RP ensemble studied above the typical value is of order $N^{-\gamma/\mu}$. Furthermore, from Eq. (C1) one has that the moments $\langle |\mathcal{H}_{ij}|^q \rangle$ diverge with N for $q > 2/p$, while in the Lévy case they diverge as soon as $q \geq \mu$.

To establish a tighter connection with the results of Refs. [58,59], one can then change the coordinates to $\gamma_{\text{eff}} = \gamma/\mu$ and $p_{\text{eff}} = 1/\mu$ [89]. In terms of these parameters, the

AL and ergodic transitions of Eqs. (5) become

$$\gamma_{\text{eff}}^{\text{ergo}} = \begin{cases} 1 & \text{for } p_{\text{eff}} \leq 1/2 \\ 2p_{\text{eff}} & \text{for } p_{\text{eff}} > 1/2, \end{cases} \quad (\text{C2})$$

$$\gamma_{\text{eff}}^{\text{AL}} = \begin{cases} 2 & \text{for } p_{\text{eff}} \leq 1 \\ 2p_{\text{eff}} & \text{for } p_{\text{eff}} > 1, \end{cases}$$

and the phase diagram of Fig. 2 transforms into the one shown in the left panel of Fig. 12. [In the coordinates $(p_{\text{eff}}, \gamma_{\text{eff}})$ the transition from the weakly ergodic phase to the fully rotational invariant GOE one occurs at $\gamma_{\text{eff}} = 2 - 2p_{\text{eff}}$ for $1/2 < p_{\text{eff}} < 1$.] This phase diagram is indeed qualitatively similar to its LN-RP counterpart [58,59], plotted in the right panel of Fig. 12 as a function of the parameters p and γ appearing in Eq. (C1). The main differences are the presence of a mobility edge for $p_{\text{eff}} > 1$ and $\gamma_{\text{eff}} < 2p_{\text{eff}}$ (i.e., $\mu < 1$ and $\gamma < 1$) separating low-energy extended states from high-energy localized states in the Lévy case [62] and possibly the fact that the weakly ergodic regime occupies a wider portion of the phase diagram of the LN-RP ensemble: In the L-RP model, the localized phase extends with increasing the tails of the distribution of the hybridization rates (i.e., decreasing μ), while in the LN-RP model the weakly ergodic phase extends upon increasing p . This comparison, together with the discussion of Appendix B, suggests that the phase boundaries of the weakly ergodic phase are in fact very sensitive to the specific form of the tails of the distributions of the off-diagonal elements.

Below we illustrate how the simple argument put forward in Sec. VI to determine the effective width of the minibands (i.e., the Thouless energy) and the fractal exponent D_1 allows one to recover the phase diagram of the LN-RP ensemble shown in the right panel of Fig 12.

Let us assume that in the NEE phase the minibands extend over N^{D_1} adjacent energy levels. A site i within a given miniband can hybridize with the other sites j of the same miniband provided that the maximum of the N^{D_1} hybridization rates \mathcal{H}_{ij} is of the order of the width of the miniband itself, N^{D_1-1} . We introduce the exponent α to parametrize the scaling of the maximum of N^{D_1} i.i.d. elements extracted from the

log-normal distribution Eq. (C1):

$$\max_{j=1,\dots,N^{D_1}} \{\mathcal{H}_{ij}\} \sim N^{-\alpha}$$

(here we only consider the leading term and neglect corrections of order $\ln N$). A simple extreme value statistics calculation yields

$$\frac{(\gamma/2 - \alpha)^2}{p\gamma} = D_1, \quad 0 \leq \alpha \leq \gamma/2.$$

In fact, this expression is correct only if the maximum is larger than the typical value of the matrix element, $\alpha < \gamma/2$. Moreover, to be in the NEE phase, in which the effective total bandwidth is dominated by the diagonal disorder and is of order W , we need to require that $\alpha > 0$.

Imposing the self-consistent condition $N^{-\alpha} \sim N^{D_1-1}$ yields a self-consistent equation for α whose solution is

$$\alpha(\gamma, p) = \frac{(1-p)\gamma - \sqrt{(1-p)^2\gamma^2 - \gamma^2 + 4p\gamma}}{2}. \quad (\text{C3})$$

(The relevant solution is the one with the minus sign since, as explained above, one has to require that $\alpha < \gamma/2$). The transition to the ergodic phase corresponds to the points where $D_1 = 1$ (i.e., $\alpha = 0$), $\gamma_{\text{ergo}} = 4p$, while the AL transition occurs when the solution of Eq. (C3) with $\alpha \geq 0$ ceases to exist:

$$\gamma_{\text{AL}} = \begin{cases} 4/(2-p) & \text{for } p \leq 1 \\ 4p & \text{for } p > 1. \end{cases} \quad (\text{C4})$$

Hence, $p > 1$ γ_{ergo} and γ_{AL} merge, the NEE disappears, and one has a discontinuous transition between the ergodic and the AL phases.

However, the expression found above for $\gamma_{\text{ergo}} = 4p$ does not give the correct result $\gamma_{\text{ergo}} \rightarrow 1$ in the Gaussian RP limit $p \rightarrow 0$. In fact, as we have already seen in the case of the Lévy-RP ensemble (see Sec. III), the extreme value statistics argument used to determine E_{Th} as the maximum hybridization gap only applies if the tails of the off-diagonal elements are fat enough, i.e., $\mu < 2$ for the L-RP case. If $\mu > 2$, instead, Eq. (4) underestimates the Thouless energy, which is alternatively given by Fermi's golden rule, $E_{\text{Th}} \sim N \langle |\mathcal{H}_{ij}|^2 \rangle_W$. Similarly, in the LN-RP case for $p < 1/2$, the width of the minibands is much larger than $N^{-\alpha}$ and is given by $E_{\text{Th}} = \Gamma_{\text{av}} \sim N^{1-\gamma(1-p)}$. Requiring that the ergodic transition occurs when the Thouless energy becomes of the order of the total spectral bandwidth, one finally gets

$$\gamma_{\text{ergo}} = \begin{cases} 1/(1-p) & \text{for } p \leq 1/2 \\ 4p & \text{for } p > 1/2. \end{cases} \quad (\text{C5})$$

Equations (C5) and (C4) are in perfect agreement with the results of Refs. [58,59], although they have been obtained with a different approach. However, the estimation of the Thouless energy given by Fermi's golden rule for $p < 1/2$ is not expected to hold for $\gamma > 2$. In fact, for $\gamma > 2$ the typical bandwidth $N[\mathcal{H}_{ij}]_{\text{typ}}^2 \sim N^{1-\gamma}$ becomes smaller than the mean-level spacing. In other words, the typical value of the matrix elements $N^{-\gamma/2}$ is much smaller than the gap between neighboring levels and the system is essentially alike a sparse graph, where most of the matrix elements are effectively equal to 0 in the thermodynamic limit. Fermi's golden rule is not

expected to provide the correct estimation of the effective bandwidth in this regime [Eqs. (8) and (9) only work for dense matrices] [90] and one should thus switch back to $E_{\text{Th}} \sim N^{-\alpha}$, with α given by Eq. (C3). (Note that the L-RP ensemble studied in the main text does not have this feature, since in this case the typical bandwidth is larger than the mean-level spacing in the whole NEE regime and becomes equal to Δ only at the AL transition.)

Hence, imposing that $E_{\text{Th}} \sim N^{D_1-1}$ one obtains an estimation of the fractal dimension D_1 for the LN-RP ensemble:

$$D_1 = \begin{cases} 2 - \gamma(1-p) & \text{for } \gamma \leq 2 \text{ and } p \leq 1/2 \\ 1 - \alpha(\gamma, p) & \text{for } \gamma > 2 \text{ or } p > 1/2. \end{cases} \quad (\text{C6})$$

The equation above predicts that the fractal dimension D_1 is equal to one at the ergodic transition and exhibits a discontinuous jump at the AL transition, which is also in agreement with the findings of Refs. [58,59]. We find, however, a different value of the jump,

$$D_1(\gamma = \gamma_{\text{AL}}) = \frac{p}{2-p},$$

which goes to zero in the RP limit $p \rightarrow 0$ and to 1 at the tricritical point $p \rightarrow 1$, but is strictly smaller than the value predicted in Ref. [59].

The fact that, different from the Lévy case, in the LN-RP ensemble the typical bandwidth is smaller than the mean-level spacing for $\gamma > 2$, results in a different fractal structure of the minibands between the two models, which is reflected in the slightly different form of the overlap correlation function $K_2(\omega)$ (see Fig. 9 and Ref. [59]).

APPENDIX D: FRACTAL DIMENSION D_2 AND THE FINITE-SIZE SCALING ANALYSIS OF THE MOMENTS OF WAVE-FUNCTION AMPLITUDES

In this Appendix, we show a few more numerical results on the fractal dimensions and on their finite-size scaling behavior.

In Fig. 13, we plot the flowing fractal exponent $D_2(N, \gamma)$ as a function of γ for three values of $\mu \in (1, 2)$ and several system sizes. $D_2(N, \gamma)$ is estimated using Eqs. (20) from the scaling with N of the IPR, and its behavior is qualitatively similar to the one of $D_1(N, \gamma)$, shown in Fig. 4.

Next we present an independent estimation of the value of the critical exponent ν_{ergo} which describes the critical scaling of the anomalous dimensions close to the transition point with the ergodic phase, $\gamma_{\text{ergo}} = 1$. This analysis is inspired by the one proposed in Ref. [11] (see also Ref. [36]) on the insulating side of the MBL transition, where the fractal dimensions are decreasing functions of the disorder. More precisely, we posit that in the NEE phase, $1 < \gamma < \mu$, the moments $\langle \Upsilon_q \rangle$ behave as

$$\begin{aligned} \langle \Upsilon_1(N, \gamma) \rangle - \langle \Upsilon_1(N, \gamma = 1) \rangle &= -D_{1,c} \frac{\ln N}{\xi(\gamma)}, \\ \langle \Upsilon_q(N, \gamma) \rangle - \langle \Upsilon_q(N, \gamma = 1) \rangle &= (q-1) D_{q,c} \frac{\ln N}{\xi(\gamma)}, \end{aligned} \quad (\text{D1})$$

with $D_{q,c}$ being the fractal dimensions at the transition point.

The length scale ξ depends on the distance to the critical point $\gamma_{\text{ergo}} = 1$ and lies in the range $(1, +\infty)$, which guarantees the fractal dimensions to remain positive. The scaling

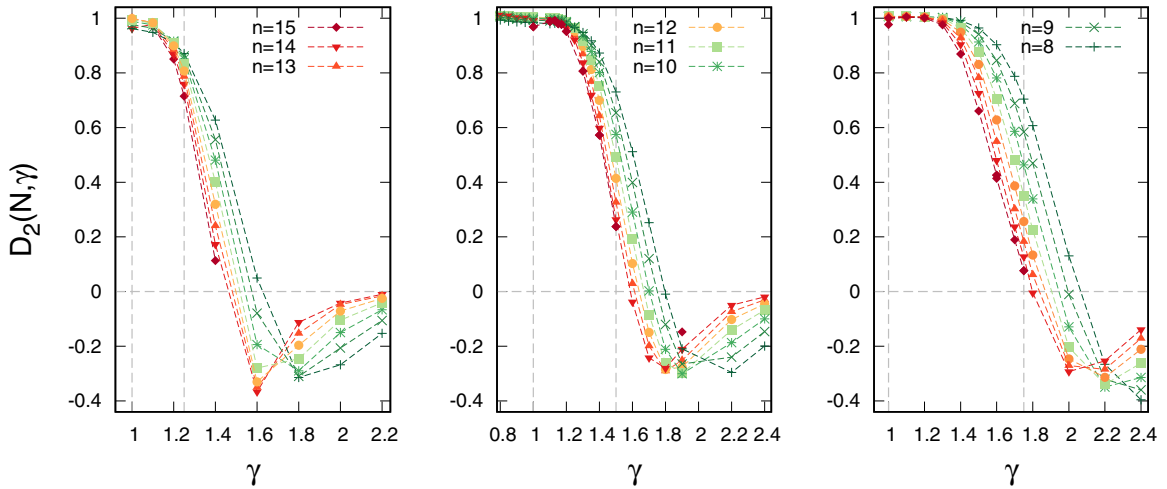


FIG. 13. Flowing N -dependent fractal dimensions $D_2(N, \gamma)$ for $\mu = 1.25$ (left), $\mu = 1.5$ (middle), $\mu = 1.75$ (right), and $N = 2^n$ with $n = 8, \dots, 15$, computed via Eqs. (20) from the scaling of the second moment of the wave functions' amplitudes measured from exact diagonalizations.

ansatz above implies that in the limit $\ln N \gg \xi$, the leading terms follow $\langle \Upsilon_1 \rangle \sim D_{1,c}(1 - 1/\xi(\gamma)) \ln N$ and $\langle \Upsilon_q \rangle \sim -(q-1)D_{q,c}(1 - 1/\xi(\gamma)) \ln N$, while in the opposite limit, $\ln N \ll \xi$, one retrieves the critical scaling. For Eqs. (6) and (7) to be satisfied, one then should have that in the NEE phase

$$\xi = \frac{\mu - 1}{\gamma - 1}. \quad (\text{D2})$$

Note that $\xi(\gamma = \mu) = 1$, in such a way that $D_q \rightarrow 0$ for $N \rightarrow \infty$ at the AL. As shown in Fig. 14, a very good data collapse is obtained in the intermediate phase $\gamma \in (1, \mu)$ and for all values of μ when the first and second moments of the wave-function amplitudes are plotted as a function of the scaling variable $\ln N/\xi$, where $\xi(\gamma)$ is chosen as in Eq. (D2), confirming that the critical exponent ν_{ergo} is equal to one at the ergodic transition independently of μ . Notice that there is no adjustable parameter in this procedure.

Note that the finite-size scaling of Fig. 14 with ξ given by Eq. (D2) automatically implies that for the L-RP model in the thermodynamic limit, $\ln N \gg \xi$, the ratio D_q/D_1 is equal to $D_{q,c}/D_{1,c}$ independently of γ . Hence, from Eq. (6) one thus has that for $1 < \mu < 2$ and $1 < \gamma < \mu$ the fractal dimensions D_q are also straight lines vanishing at $\gamma = \mu$ with q -dependent slopes: $D_q(\gamma) = D_{q,c}(\mu - \gamma)/(\mu - 1)$. This is fully consis-

tent with our prediction Eq. (7), with $D_{\infty,c} = 2(\mu - 1)/\mu$. If $\ln N \ll \xi$, however, one does not observe that the ratio D_q/D_1 is constant due to the fact that the scaling functions for different values of q are different, producing different q -dependent finite-size effects (see Fig. 5).

This is confirmed by Fig. 15, where we plot the same finite-size scaling analysis for different moments of the wave functions' amplitudes and for $\mu = 1.75$, showing that a very good collapse is found for all values of q in terms of the scaling variable $\ln N/\xi$. The scaling functions depend on q and the fact that the scaling function for $q \rightarrow \infty$ approaches a straight line for $\ln N/\xi \gg 1$ with a smaller slope compared to the scaling function for $q = 1$ indicates that $D_{\infty,c} < D_{1,c}$, in agreement with the fact that D_∞ has a discontinuous jump at the ergodic transition.

APPENDIX E: PERTURBATION THEORY AND THE SPECTRUM OF FRACTAL DIMENSIONS IN THE AL PHASE

In this Appendix, we discuss the standard perturbation theory for the amplitudes $w_{ij} = |\psi_i(j)|^2$, focusing in particular on its domain of convergence. This calculation allows one to obtain the full spectrum of fractal dimensions in the AL phase

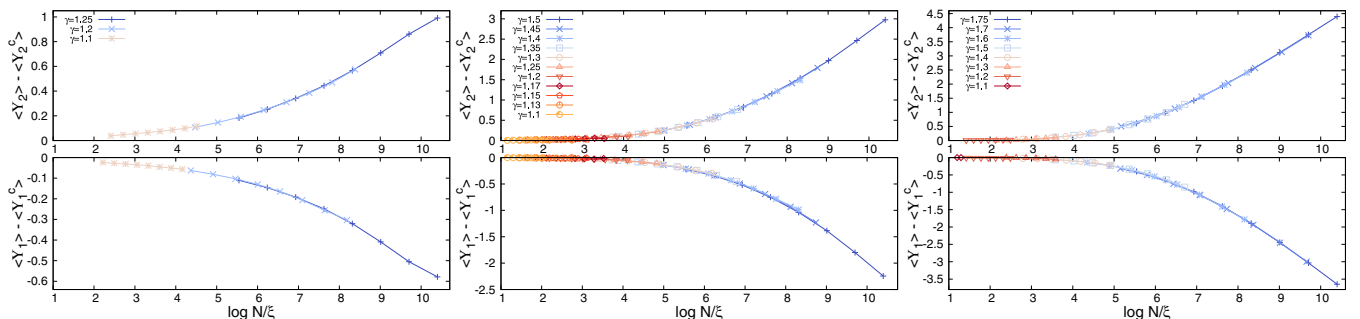


FIG. 14. Scaling curves for the first (bottom) and second (top) moments of the wave-function amplitudes varying $\gamma \in (1, \mu)$ in the NEE phase for $\mu = 1.25$ (left), $\mu = 1.5$ (middle), and $\mu = 1.75$ (right) according to Eqs. (D1) and with ξ given by Eq. (D2).

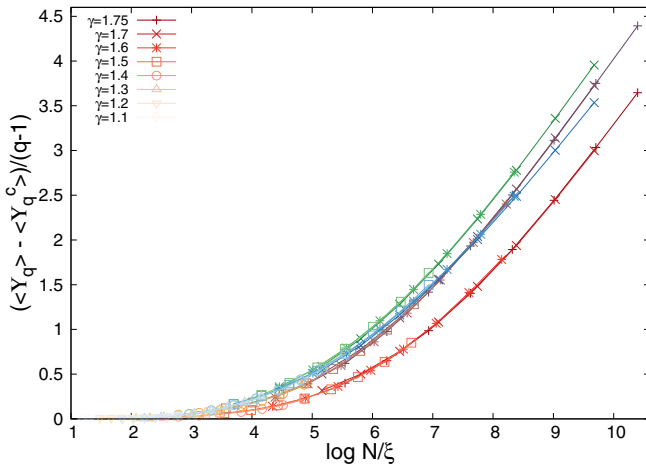


FIG. 15. Scaling curves for the q th moments of the wavefunction amplitudes (divided by $q - 1$) varying $\gamma \in (1, \mu)$ in the NEE phase for $\mu = 1.75$ according to Eqs. (D1) and with ξ given by Eq. (D2), for $q = 1$ (red), $q = 2$ (brown), $q = 6$ (green), and $q \rightarrow \infty$ (blue). For $q = 1$, we have changed the signs of Υ_1 to have all the data on the positive side of the y axis.

where the perturbative expansion converges absolutely. We focus on the region $\mu < 2$, since the case $\mu > 2$ is equivalent to the RP ensemble treated in Ref. [44].

The first-order perturbation theory gives

$$|\psi_i\rangle = |i\rangle + \sum_{j(\neq i)} \frac{\mathcal{L}_{ij}}{\epsilon_i - \epsilon_j} |j\rangle.$$

The amplitude on the sites $j \neq i$ is therefore given by

$$w_{ij} = \frac{\mathcal{L}_{ij}^2}{(\epsilon_i - \epsilon_j)^2} \equiv R_{ij}^2, \quad (\text{E1})$$

where $R_{ij} = \mathcal{L}_{ij}/\delta_{ij}$ are the hybridization ratios between the levels i and j (with $\delta_{ij} \equiv \epsilon_i - \epsilon_j$). The typical value of R_{ij} is

$$R_{ij}^{\text{typ}} = \frac{\mathcal{L}_{ij}^{\text{typ}}}{\delta_{ij}^{\text{typ}}} \sim \frac{N^{-\gamma/\mu}}{W} \rightarrow 0.$$

However, large hybridization ratios can be obtained from the biggest off-diagonal coupling:

$$R_{ij}^{\text{max}} = \frac{\mathcal{L}_{ij}^{\text{max}}}{\delta_{ij}^{\text{typ}}} \sim \frac{N^{(1-\gamma)/\mu}}{W},$$

which vanish in the thermodynamic limit for $\gamma > 1$.

Finally, large hybridization ratios can be obtained from small energy differences (i.e., consecutive levels),

$$R_{ij}^{\text{next}} = \frac{\mathcal{L}_{ij}^{\text{typ}}}{\delta_{ij}^{\text{min}}} \sim \frac{N^{-\gamma/\mu}}{WN^{-1}} \sim N^{1-\gamma/\mu},$$

which vanish in the thermodynamic limit for $\gamma > \mu$. As a result, the perturbative series converges absolutely for $\mu > 1$ and $\gamma > \mu$, and for $\mu < 1$ and $\gamma > 1$, as indicated in Fig. 2, since the average off-diagonal matrix elements times the coordination number N is much smaller than the typical difference of the diagonal matrix elements [recovering the Mott's criterion Eq. (8)]. For $\mu > 1$ and $\gamma < \mu$, the convergence of the

series might still occur because of the random and independently fluctuating signs of \mathcal{L}_{ij} and δ_{ij} , as in the RP model with Gaussian elements. To analyze this possibility, we perform the calculation at second order, which gives

$$w_{ij} \approx \delta_{ij} + \frac{1}{\epsilon_i - \epsilon_j} \left[\mathcal{L}_{ij} + \sum_{k \neq i} \frac{\mathcal{L}_{jk} \mathcal{L}_{ki}}{\epsilon_i - \epsilon_k} + \dots \right].$$

Since $\mathcal{L}_{jk} \mathcal{L}_{ki}$ is the product of two uncorrelated Lévy-distributed random variables, we can apply the generalized central limit theorem to characterize the probability distribution of the sum in the square brackets, which is again a Lévy distributed random variable with exponent $1 + \mu$ and typical value of order $N^{1-2\gamma/\mu}$.

For $\mu > 1$, the typical value dominates the average, in agreement with the arguments given in Sec. IV. (For $\mu < 1$ instead this term is of order $N \langle \mathcal{L}_{ij} \rangle_W^2 \sim N^{1-2\gamma}$.) This term is much bigger than the typical value of the first term, $N^{-\gamma/\mu}$, if $\gamma < \mu$. By applying the same kind of reasoning, it is straightforward to generalize this calculation to the higher order terms of the perturbative expansion, showing that the terms of order n in the square brackets above are Lévy-distributed random variables with exponent $1 + \mu$ and typical value scaling as $N^{n-1} (\langle \mathcal{L}_{ij} \rangle_W)^n \sim N^{n(1-\gamma/\mu)-1}$ for $\mu > 1$. (For $\mu < 1$ instead, this term scales as $N^{n(1-\gamma)-1}$.) Note that in the RP limit, $\mu > 2$, the higher order terms are instead negligible in the thermodynamic limit thanks to the random signs of the matrix elements which ensure that $\langle \mathcal{L}_{jk} \mathcal{L}_{ki} \rangle = 0$, implying that the first-order computation gives the correct results at large N in the Gaussian case.

It is also instructive to analyze the perturbative expansions for the eigenvalues, which read

$$\lambda_i \approx \epsilon_i + \sum_{j \neq i} \frac{\mathcal{L}_{ij}^2}{\epsilon_i - \epsilon_j} + \sum_{j \neq i} \sum_{k \neq i} \frac{\mathcal{L}_{ij} \mathcal{L}_{jk} \mathcal{L}_{ki}}{(\epsilon_i - \epsilon_j)(\epsilon_i - \epsilon_k)} \dots$$

The second term of the right hand side of the expression above is a Lévy-distributed random variable with power-law exponent $1 + \mu/2$ and typical value of order $N^{1-2\gamma/\mu}$. By applying the arguments of Sec. IV, one obtains that, due to the power-law tails of the distribution, the average amount of energy that the levels move at second order is $N \langle \mathcal{L}_{ij}^2 \rangle_W = N^{1-\gamma}$ (where the average is cut at the spectral bandwidth). Note that, differently from the RP model, $N \langle \mathcal{L}_{ij}^2 \rangle_W \neq N \langle \mathcal{L}_{ij} \rangle_W^2$, implying that the typical and the average bandwidth do not coincide. The amplitude of higher order terms can be evaluated as above. At order n , one has $N^{n-1} (\langle \mathcal{L}_{ij} \rangle_W)^n \sim N^{n(1-\gamma/\mu)-1}$ for $\mu > 1$.

1. The NEE phase

Hence, due to the fat-tails distribution of the off-diagonal matrix elements, differently from its Gaussian RP counterpart, in the L-RP ensemble the higher order terms of the perturbative series cannot be neglected in the NEE regime $1 < \mu < 2$ and $\gamma < \mu$. In the following, we show that, in fact, keeping only the first-order term leads to a wrong result for the probability distribution of the wave functions' amplitudes and the anomalous dimensions.

At first order, Eq. (E1), the w_{ij} 's are given by the product of two power-law distributed random variables: $x_{ij} = \mathcal{L}_{ij}^2$ have a power-law tail with an exponent $1 + \mu/2$ and typical value

$N^{-2\gamma/\mu}$,

$$P(x_{ij}) = \frac{\mu}{2N^\gamma x_{ij}^{1+\mu/2}} \theta(x_{ij} > N^{-2\gamma/\mu}),$$

and $y_{ij} = \delta_{ij}^{-2}$ have typical value of $O(W)$ and power-law tails with an exponent $3/2$:

$$P(y_{ij}) = \frac{e^{-1/(4W^2 y_{ij})}}{\sqrt{4\pi W^2}} y_{ij}^{-3/2}.$$

For $\mu > 1$, the amplitudes w_{ij} are power-law distributed with an exponent $3/2$ and typical value $w_{ij}^{\text{typ}} = x_{ij}^{\text{typ}} y_{ij}^{\text{typ}} = N^{-2\gamma/\mu}$. Without loss of generality, the distribution can be written as

$$P(w_{ij}) = \frac{1}{w_{ij}^{\text{typ}}} P_{\text{reg}}\left(\frac{w_{ij}}{w_{ij}^{\text{typ}}}\right) + c \frac{\theta(w_{ij} > w_{ij}^{\text{typ}})}{N^{\gamma/\mu} w_{ij}^{3/2}}.$$

The normalization of wave functions imposes that $\langle w_{ij} \rangle = N^{-1}$, which implies an upper cutoff w_{ij}^{max} to the singular part of the distribution above,

$$N \langle w_{ij} \rangle \sim N^{1-2\gamma/\mu} + \frac{c}{N^{\gamma/\mu-1}} \int_{N^{-2\gamma/\mu}}^{w_{ij}^{\text{max}}} w_{ij}^{-1/2} dw_{ij} = 1,$$

which yields

$$w_{ij}^{\text{max}} \sim N^{2(\gamma/\mu-1)}.$$

A caution, however, should be taken, since the amplitudes w_{ij} on any lattice site cannot exceed 1. Hence, the above estimation of w_{ij}^{max} is only correct if $2(\gamma/\mu - 1) < 0$, i.e., $\gamma < \mu$, while for $\gamma > \mu$ we have that $w_{ij}^{\text{max}} = 1$. To compensate for the deficiency of normalization of $\langle w \rangle$ in the latter case, one has to assume a singular part of the distribution:

$$\hat{P}(w_{ij}) = P(w_{ij}) + A\delta(w_{ij} - 1).$$

One can see that for $\gamma > \mu$ the average $\langle w \rangle$ is dominated by the singular term and $A = N^{-1}$. This corresponds to the strongly localized wave functions $\psi_i(j)$ on site i .

At this point, one can easily compute the spectrum of fractal dimensions $f(\alpha)$, describing the number of amplitudes scaling as $N^{-\alpha}$. For $\gamma < \mu$, we have

$$N^{f(\alpha)} = \frac{c}{N^{\gamma/\mu-1}} \int_{N^{-\alpha}}^{N^{2(\gamma/\mu-1)}} w_{ij}^{-3/2} dw_{ij} \sim N^{\alpha/2-\gamma/\mu+1},$$

for $2(1 - \gamma/\mu) = \alpha_{\min} < \alpha < \alpha_{\max} = 2\gamma/\mu$, which gives

$$f(\alpha) = \frac{\alpha}{2} - \frac{\gamma}{\mu} + 1 \quad (\alpha_{\min} < \alpha < \alpha_{\max}).$$

In the localized region $\gamma > \mu$, $\alpha_{\min} = 0$. At the AL transition point, the function $f(\alpha) = \alpha/2$ has the same triangular shape

as the Anderson model on the Bethe lattice at the localization transition. In the region of the extended nonergodic states, $1 < \gamma < \mu$, $\alpha_{\min} > 0$.

Alternatively, one can compute directly the moments $N \langle |\psi_i(j)|^{2q} \rangle \sim N^{-\tau_q}$:

$$\langle w^q \rangle \sim N^{-2q\gamma/\mu} + \frac{c}{N^{\gamma/\mu}} \int_{N^{-2\gamma/\mu}}^{N^{2(\gamma/\mu-1)}} w_{ij}^{q-3/2} dw_{ij}.$$

For $q < 1/2$, the moments $\langle w^q \rangle$ are dominated by the typical values and $\tau_q = 2q\gamma/\mu - 1$, while for $q > 1/2$ the moments are dominated by the upper cutoff and $\tau_q = 2(q-1)(1 - \gamma/\mu)$. One can thus compute the fractal dimensions $D_q = \tau_q/(q-1)$:

$$D_q = \begin{cases} 2(1 - \gamma/\mu) & \text{for } q > 1/2 \\ \frac{1-2q\gamma/\mu}{1-q} & \text{for } q < 1/2. \end{cases} \quad (\text{E2})$$

Thus the first-order expression does not coincide with the one found in the main text, Eq. (6), and corresponds to NEE states for $1 < \gamma < \mu$ that occupy a fraction $N^{1-2\gamma/\mu}$ of sites only. This is due to the fact that the first-order computation neglects the effect of anomalously large matrix elements that can hybridize sites at an energy distance much larger than $N[\mathcal{H}_{ij}^2]_{\text{typ}}$. The main difference is that the first-order calculation predicts that D_q approaches a value smaller than one, $D_c = 2(1 - 1/\mu)$, at the ergodic transition $\gamma_{\text{ergo}} = 1$ for all $q > 1/2$, where $D_c = 2(1 - 1/\mu)$, with a discontinuous jump at the transition. This also predicts that, as for the RP model, the fractal dimensions are degenerate.

2. The localized phase

In the localized phase, $\gamma > \mu$, the perturbative expansion does converge. Repeating the calculation above, one obtains the spectrum of fractal dimensions as [53]

$$D_q = \begin{cases} 0 & \text{for } q > \mu/(2\gamma) \\ \frac{1-2q\gamma/\mu}{1-q} & \text{for } q < \mu/(2\gamma). \end{cases} \quad (\text{E3})$$

A similar behavior is also found for the Anderson model on the Bethe lattice.

For $\mu < 1$ and $\gamma > 1$, going back to Eq. (E1) one has that at first order in perturbation theory, the amplitudes w_{ij} are power-law distributed with an exponent $1 + \mu/2$ and typical value $w_{ij}^{\text{typ}} = x_{ij}^{\text{typ}} y_{ij}^{\text{typ}} = N^{-2\gamma/\mu}$:

$$P(w_{ij}) = \frac{1}{w_{ij}^{\text{typ}}} P_{\text{reg}}\left(\frac{w_{ij}}{w_{ij}^{\text{typ}}}\right) + c \frac{\theta(w_{ij} > w_{ij}^{\text{typ}})}{N^\gamma w_{ij}^{1+\mu/2}}.$$

The computation for the moments of the wave functions's amplitudes thus yields that the spectrum of fractal dimensions is the one given by Eq. (E3).

- [1] F. Wegner, *Z. Phys. B* **36**, 209 (1980).
- [2] A. Rodriguez, L. J. Vasquez, K. Slevin, and R. A. Romer, *Phys. Rev. B* **84**, 134209 (2011).
- [3] D. M. Basko, I. L. Aleiner, and B. L. Altshuler, *Ann. Phys.* **321**, 1126 (2006).
- [4] I. V. Gornyi, A. D. Mirlin, and D. G. Polyakov, *Phys. Rev. Lett.* **95**, 206603 (2005).

- [5] E. Altman and R. Vosk, *Annu. Rev. Condens. Matter Phys.* **6**, 383 (2015).
- [6] R. Nandkishore and D. A. Huse, *Annu. Rev. Condens. Matter Phys.* **6**, 15 (2015).
- [7] D. A. Abanin and Z. Papić, *Ann. Phys.* **529**, 1700169 (2017).
- [8] F. Alet and N. Laflorencie, *C. R. Phys.* **19**, 498 (2018).

- [9] D. A. Abanin, E. Altman, I. Bloch, and M. Serbyn, *Rev. Mod. Phys.* **91**, 021001 (2019).
- [10] D. J. Luitz, N. Laflorencie, and F. Alet, *Phys. Rev. B* **93**, 060201(R) (2016).
- [11] N. Macé, F. Alet, and N. Laflorencie, *Phys. Rev. Lett.* **123**, 180601 (2019).
- [12] F. Pietracaprina and N. Laflorencie, [arXiv:1906.05709](https://arxiv.org/abs/1906.05709).
- [13] G. De Tomasi, I. M. Khaymovich, F. Pollmann, and S. Warzel, [arXiv:2011.03048](https://arxiv.org/abs/2011.03048)
- [14] I. V. Gornyi, A. D. Mirlin, D. G. Polyakov, and A. L. Burin, *Ann. Phys.* **529**, 1600360 (2017);
- [15] K. S. Tikhonov and A. D. Mirlin, *Phys. Rev. B* **97**, 214205 (2018).
- [16] M. Tarzia, *Phys. Rev. B* **102**, 014208 (2020).
- [17] D. J. Luitz and Y. Bar Lev, *Ann. Phys.* **529**, 1600350 (2017).
- [18] K. Agarwal, E. Altman, E. Demler, S. Gopalakrishnan, D. A. Huse, and M. Knap, *Ann. Phys.* **529**, 1600326 (2017).
- [19] G. Biroli and M. Tarzia, *Phys. Rev. B* **96**, 201114(R) (2017).
- [20] B. L. Altshuler, Y. Gefen, A. Kamenev, and L. S. Levitov, *Phys. Rev. Lett.* **78**, 2803 (1997).
- [21] L. Faoro, M. V. Feigel'man, and L. Ioffe, *Ann. Phys.* **409**, 167916 (2019).
- [22] C. L. Baldwin and C. R. Laumann, *Phys. Rev. B* **97**, 224201 (2018).
- [23] V. Smelyanskiy, K. Kechedzhi, S. Boixo, H. Neven, and B. Altshuler, [arXiv:1907.01609](https://arxiv.org/abs/1907.01609)
- [24] T. Parolini and G. Mossi, [arXiv:2007.00315](https://arxiv.org/abs/2007.00315)
- [25] G. Biroli, D. Facoetti, M. Schiró, M. Tarzia, and P. Vivo, *Phys. Rev. B* **103**, 014204 (2021)
- [26] C. Monthus and T. Garel, *J. Phys. A: Math. Theor.* **44**, 145001 (2011).
- [27] K. S. Tikhonov and A. D. Mirlin, *Phys. Rev. B* **94**, 184203 (2016); M. Sonner, K. S. Tikhonov, and A. D. Mirlin, *ibid.* **96**, 214204 (2017).
- [28] G. Biroli, M. Tarzia, *Phys. Rev. B* **102**, 064211 (2020).
- [29] A. De Luca, B. L. Altshuler, V. E. Kravtsov, and A. Scardicchio, *Phys. Rev. Lett.* **113**, 046806 (2014); A. De Luca, A. Scardicchio, V. E. Kravtsov, and B. L. Altshuler, [arXiv:1401.0019](https://arxiv.org/abs/1401.0019).
- [30] B. L. Altshuler, E. Cuevas, L. B. Ioffe, and V. E. Kravtsov, *Phys. Rev. Lett.* **117**, 156601 (2016); B. L. Altshuler, L. B. Ioffe, and V. E. Kravtsov, [arXiv:1610.00758](https://arxiv.org/abs/1610.00758).
- [31] V. E. Kravtsov, B. L. Altshuler, and L. B. Ioffe, *Ann. Phys.* **389**, 148 (2018).
- [32] S. Bera, G. De Tomasi, I. M. Khaymovich, and A. Scardicchio, *Phys. Rev. B* **98**, 134205 (2018).
- [33] G. De Tomasi, S. Bera, A. Scardicchio, and I. M. Khaymovich, *Phys. Rev. B* **101**, 100201(R) (2020).
- [34] S. Savitz, C. Peng, and G. Refael, *Phys. Rev. B* **100**, 094201 (2019).
- [35] K. S. Tikhonov, A. D. Mirlin, and M. A. Skvortsov, *Phys. Rev. B* **94**, 220203(R) (2016).
- [36] I. Garcia-Mata, O. Giraud, B. Georgeot, J. Martin, R. Dubertrand, and G. Lemarié, *Phys. Rev. Lett.* **118**, 166801 (2017).
- [37] G. Biroli and M. Tarzia, [arXiv:1810.07545](https://arxiv.org/abs/1810.07545)
- [38] K. S. Tikhonov and A. D. Mirlin, *Phys. Rev. B* **99**, 024202 (2019).
- [39] K. Kechedzhi, V. N. Smelyanskiy, J. R. McClean, V. S. Denchev, M. Mohseni, S. V. Isakov, S. Boixo, B. L. Altshuler, and H. Neven, [arXiv:1807.04792](https://arxiv.org/abs/1807.04792)
- [40] M. Pino, L. B. Ioffe, and B. L. Altshuler, *PNAS* **113**, 536 (2016); M. Pino, V. E. Kravtsov, B. L. Altshuler, and L. B. Ioffe, *Phys. Rev. B* **96**, 214205 (2017).
- [41] T. Micklitz, F. Monteiro, and A. Altland, *Phys. Rev. Lett.* **123**, 125701 (2019); F. Monteiro, T. Micklitz, M. Tezuka, and A. Altland, *Phys. Rev. Research* **3**, 013023 (2021)
- [42] M. L. Metha, *Random Matrices*, 3rd ed. (Elsevier, Amsterdam, 2004).
- [43] *The Oxford Handbook of Random Matrix Theory*, edited by G. Akemann, J. Baik, and P. Di Francesco (Oxford University Press, Oxford, 2011).
- [44] V. E. Kravtsov, I. M. Khaymovich, E. Cuevas, and M. Amini, *New J. Phys.* **17**, 122002 (2015).
- [45] N. Rosenzweig and C. E. Porter, *Phys. Rev.* **120**, 1698 (1960).
- [46] P. von Soosten and S. Warzel, *Lett. Math. Phys.* **109**, 905 (2019).
- [47] D. Facoetti, P. Vivo, and G. Biroli, *Europhys. Lett.* **115**, 47003 (2016).
- [48] E. Bogomolny and M. Sieber, *Phys. Rev. E* **98**, 042116 (2018).
- [49] G. de Tomasi, M. Amini, S. Bera, I. M. Khaymovich, and V. E. Kravtsov, *SciPost Phys.* **6**, 014 (2019).
- [50] M. Pino, J. Tabanera, and P. Serna, *J. Phys. A: Math. Theor.* **52**, 475101 (2019).
- [51] K. Truong and A. Ossipov, *Europhys. Lett.* **116**, 37002 (2016).
- [52] M. Amini, *Europhys. Lett.* **117**, 30003 (2017).
- [53] C. Monthus, *J. Phys. A* **50**, 295101 (2017).
- [54] P. Shukla, *New J. Phys.* **18**, 021004 (2016).
- [55] A. Altland, M. Janssen, and B. Shapiro, *Phys. Rev. E* **56**, 1471 (1997).
- [56] H. Kunz and B. Shapiro, *Phys. Rev. E* **58**, 400 (1998).
- [57] S. Roy and D. E. Logan, *Phys. Rev. B* **101**, 134202 (2020).
- [58] V. E. Kravtsov, I. M. Khaymovich, B. L. Altshuler, and L. B. Ioffe [arXiv:2002.02979](https://arxiv.org/abs/2002.02979)
- [59] I. M. Khaymovich, V. E. Kravtsov, B. L. Altshuler, and L. B. Ioffe, *Phys. Rev. Research* **2**, 043346 (2020).
- [60] P. A. Nosov, I. M. Khaymovich, and V. E. Kravtsov, *Phys. Rev. B* **99**, 104203 (2019).
- [61] P. Cizeau and J.-P. Bouchaud, *Phys. Rev. E* **50**, 1810 (1994).
- [62] E. Tarquini, G. Biroli, and M. Tarzia, *Phys. Rev. Lett.* **116**, 010601 (2016).
- [63] G. Ben Arous and A. Guionnet, *Comm. Math. Phys.* **278**, 715 (2008).
- [64] Z. Burda, J. Jurkiewicz, M. A. Nowak, G. Papp, and I. Zahed, *Phys. Rev. E* **75**, 051126 (2007).
- [65] F. L. Metz, I. Neri, and D. Bollè, *Phys. Rev. E* **82**, 031135 (2010); *J. Stat. Mech.* (2010) P01010.
- [66] C. Monthus, *J. Stat. Mech.* (2016) 093304.
- [67] G. Biroli, J.-P. Bouchaud, and M. Potters, *Europhys. Lett.* **78**, 10001 (2007).
- [68] A. Auffinger, G. Ben Arous, and S. Péché, *Ann. Inst. H. Poincaré Probab. Statist.* **45**, 589 (2009).
- [69] C. Bordenave and A. Guionnet, *Probab. Theory and Relat. Fields* **157**, 885 (2013).
- [70] S. Majumdar, G. Schehr, D. Villamaina, and P. Vivo, *J. Phys. A* **46**, 022001 (2013).

- [71] For concreteness, one can take $p(\epsilon) = e^{-\epsilon^2/(2W^2)}/\sqrt{2\pi W^2}$ or a box distribution in the interval $[-W/2, W/2]$, with W of order 1.
- [72] A. Aggarwal, P. Lopatto, H. T. Yau, [arXiv:1806.07363](#)
- [73] A. Aggarwal, P. Lopatto, and J. Marcinek, [arXiv:2002.09355](#)
- [74] R. Abou-Chacra, P. W. Anderson, and D. J. Thouless, *J. Phys. C* **6**, 1734 (1973).
- [75] Y. V. Fyodorov and A. D. Mirlin, *J. Phys. A* **24**, 2219 (1991); *Phys. Rev. Lett.* **67**, 2049 (1991); Y. V. Fyodorov, A. D. Mirlin, and H.-J. Sommers, *J. Phys. I* **2**, 1571 (1992).
- [76] In fact, for $\mu < 1$ the fractal dimension D_1 is expected to exhibit a discontinuous jump at the AL transition from $D_1 = 1$ for $\gamma \leq 1$ to $D_1 = 0$ for $\gamma > 1$ at small energy $|E| < E_{\text{loc}}(\mu, \gamma) = E_{\text{loc}}(\mu)N^{(1-\gamma)/\mu}$. At high energy, $|E| > E_{\text{loc}}(\mu, \gamma) = E_{\text{loc}}(\mu)N^{(1-\gamma)/\mu}$, instead, one has a discontinuous transition at $\gamma = 1$ between two different AL phases and D_1 should display a discontinuous jump from $D_1(\mu, E)$ for $\gamma \leq 1$ to $D_1 = 0$ for $\gamma > 1$.
- [77] V. E. Kravtsov and A. D. Mirlin, *JETP Lett.* **60**, 656 (1994).
- [78] Y. V. Fyodorov and A. D. Mirlin, *Phys. Rev. B* **51**, 13403 (1995).
- [79] The prefactor N^{D_1} is such that for $\eta = N^{-1}$ one has $\text{Im}\mathcal{G}_{\text{typ}} = N^{D_1-1}$ matching the regime $N^{-1} \ll \eta \ll E_{\text{Th}}$ of Eq. (17).
- [80] V. Oganessian and D. A. Huse, *Phys. Rev. B* **75**, 155111 (2007).
- [81] B. L. Altshuler and B. I. Shklovskii, *Zh. Eksp. Teor. Fiz.* **91**, 220 (1986) [*JETP* **64**, 127 (1986)].
- [82] J. T. Chalker, *Physica A* **167**, 253 (1990); J. T. Chalker and G. J. Daniell, *Phys. Rev. Lett.* **61**, 593 (1988).
- [83] E. Cuevas and V. E. Kravtsov, *Phys. Rev. B* **76**, 235119 (2007).
- [84] A. D. Mirlin, *Phys. Rep.* **326**, 259 (2000).
- [85] M. Serbyn, Z. Papic', and D. A. Abanin, *Phys. Rev. B* **96**, 104201 (2017).
- [86] D. Sels and A. Polkovnikov, [arXiv:2009.04501](#)
- [87] K. S. Tikhonov and A. D. Mirlin, *Phys. Rev. B* **103**, 064204 (2021)
- [88] In the calculation of $K_2(\omega)$ with the cavity approach, the imaginary regulator η is set equal to $1/N$.
- [89] V. E. Kravtsov and I. M. Khaymovich (private communication).
- [90] Take, for instance, L-RP matrices with $\mu < 1$ and $\gamma \leq 1$, i.e., typical value $[\mathcal{H}_{ij}]_{\text{typ}} \sim N^{-\gamma/\mu}$ much smaller than the mean-level spacing $\Delta \sim N^{(1-\mu-\gamma)/\mu}$. In this case, Fermi's golden rule would suggest that the system is ergodic, since $N\langle |\mathcal{H}_{ij}|^2 \rangle_B \sim N^{2(1-\gamma)/\mu}$ diverges, while one knows from Ref. [62] that a mobility edge appears at energy E_{loc} . This is due to the fact that in this regime the system is more similar to a sparse random graph rather than to a dense random matrix.